Optics of Marine Particles

Dariusz Stramski

Scripps Institution of Oceanography
University of California San Diego
Email: dstramski@ucsd.edu

Sixth IOCCG Summer Lecture Series
4 - 16 November 2024, Hyderabad, India

Seawater is a complex optical medium with a great variety of particle types and soluble species

- Molecular water
- Inorganic salts
- Dissolved organic matter

Suspended Particulate Matter

- Plankton microorganisms
- Organic detrital particles
- Mineral particles
- Colloidal particles
- Air bubbles

A great variety of biological and mineral particle types which absorb and scatter light differently

Mineral particles

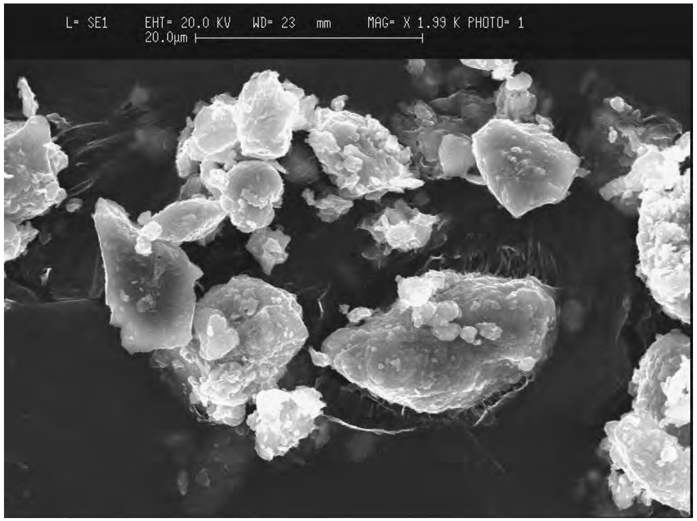

Plankton microorganisms

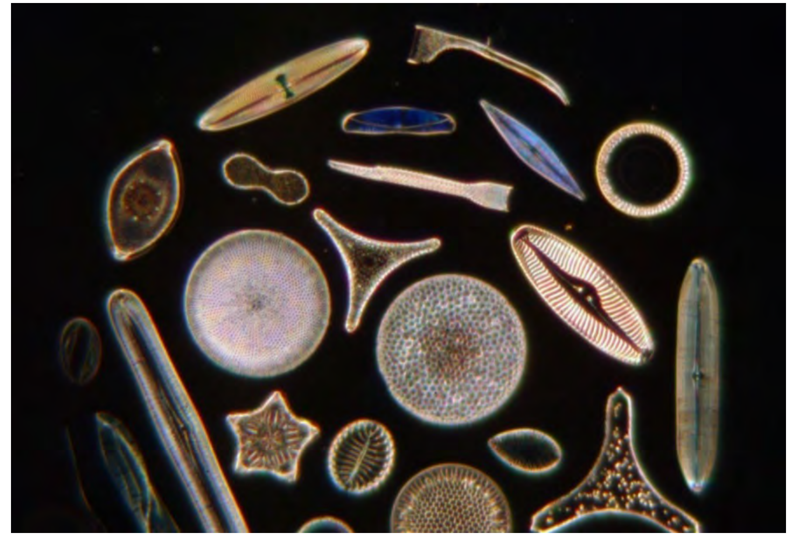

Colloids / nanoparticles

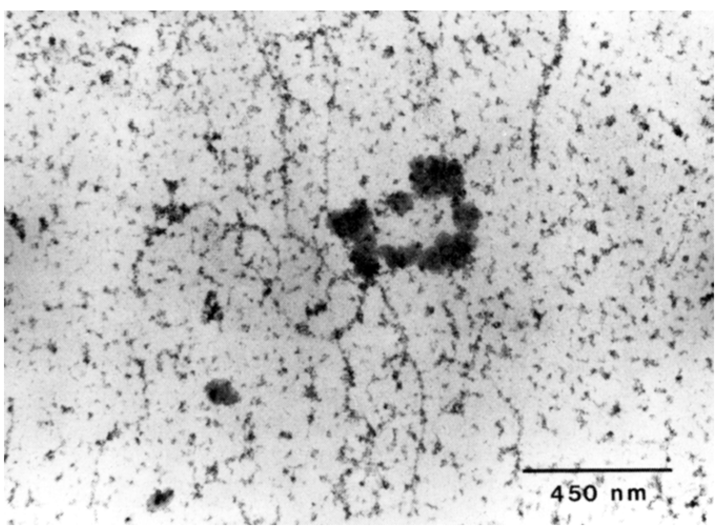

Fundamentals of single-particle optics and the linkage between the single-particle and bulk optical properties of particle suspension

Linkage between the single-particle optical properties and bulk optical properties of particle suspension

This is an example relationship for light absorption properties assuming that the bulk absorption coefficient represents a collection of identical particles (similar relationships can be written for light scattering and attenuation properties)

$$a = (N/V)\, Q_a\, G = (N/V)\, \sigma_a \qquad \sigma_a = a\,/\,(N/V)$$

Bulk properties:

a is the bulk absorption coefficient of a collection of identical particles in aqueous suspension (units of m^{-1})

N/V is the number of particles per unit volume of water (units of m^{-3})

Single-particle properties:

Q_a is the absorption efficiency factor (dimensionless) – defined on the next slide

σ_a (= $Q_a\, G$) is the absorption cross-section (units of m^2)

G is the area of geometric cross-section of particle (units of m^2)
For spherical particle $G = (\pi/4)D^2$ where D is a diameter

Note: a, Q_a, and σ_a are the spectral quantities (i.e., they are functions of light wavelength λ)

Absorption efficiency factor for a single particle

$$Q_a(\lambda) = F_a(\lambda) \, / \, F_o(\lambda)$$

$F_o(\lambda)$ - spectral radiant power intercepted by geometrical cross-section of particle

$F_a(\lambda)$ - spectral radiant power absorbed by particle

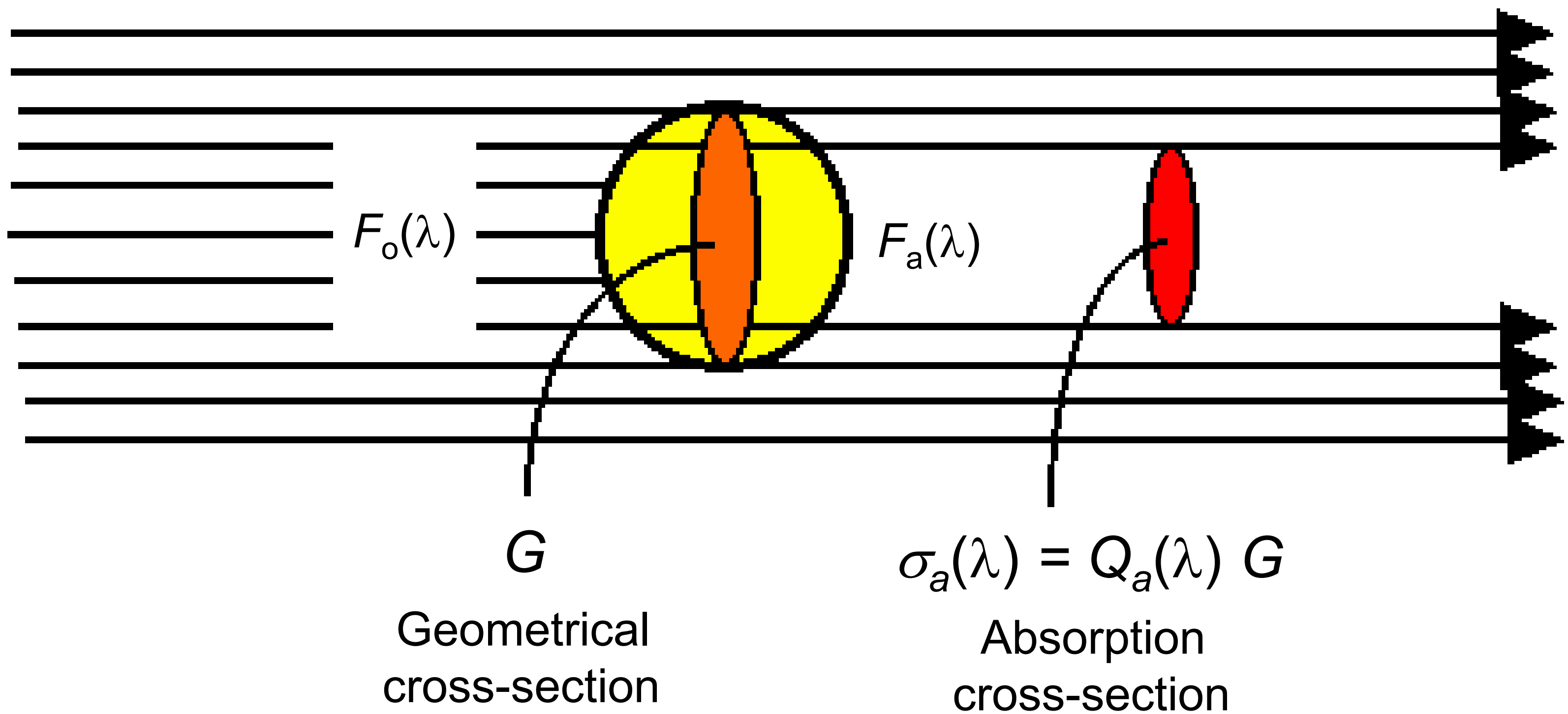

Theoretical dependence of absorption efficiency on particle properties parameterized in terms of "absorption thickness" ρ'

For a particle suspended in water

$\rho' = 4\,\alpha\, n' = a_s\, D$

where the particle size parameter α is

$\alpha = (\pi\, D\, n_w) / \lambda$

$\lambda_w = \lambda / n_w$

and the imaginary index of refraction of particle is

$n' = (a_s\, \lambda) / (4\, \pi\, n_w)$

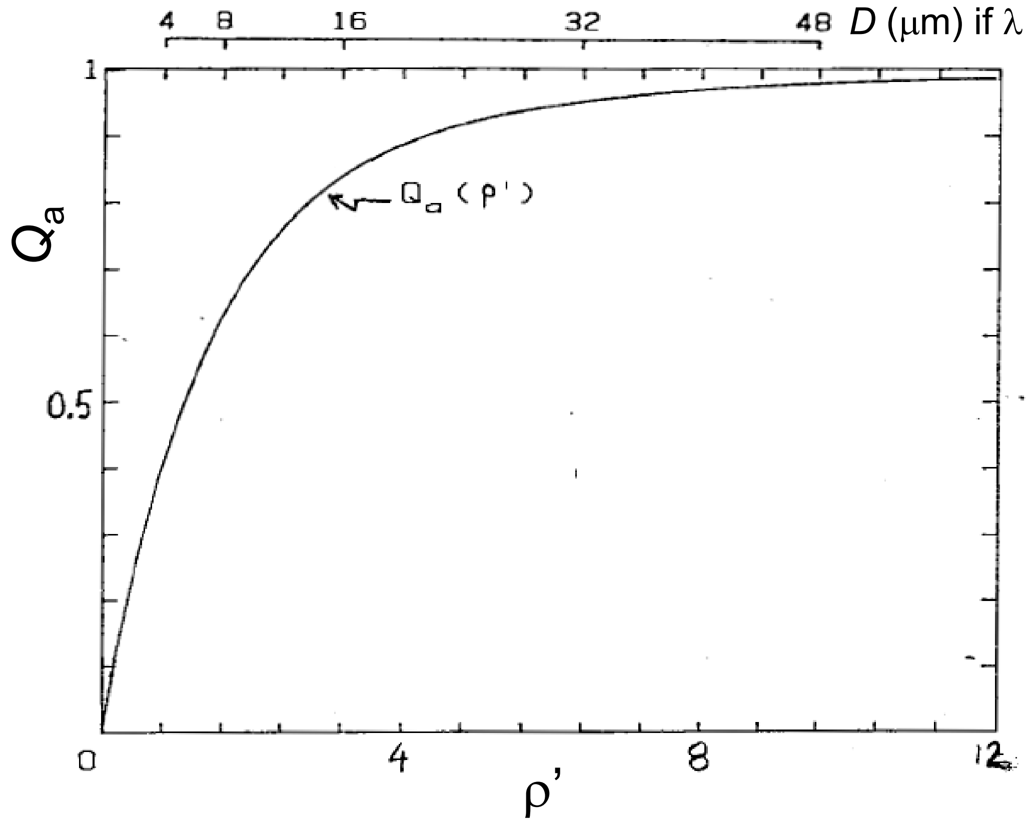

$a_s(430)$= $2 \times 10^5\ m^{-1}$ for typical phytoplankton cell

a_s (m^{-1}) is the absorption coefficient of substance forming the particle; D (m) is the particle diameter; and n_w is the refractive index of water

Note: ρ', α and n' are dimensionless; symbol x is often used in literature instead of α
Q_a, a_s, and n' are all functions of λ

(Morel and Bricaud 1981)

Example spectra of absorption efficiency factor for two phytoplankton species derived from laboratory measurements of $a(\lambda)$ and cell size distribution made on cultures

The *mean* efficiency factor, $\overline{Q_a}$, represents an "*average"* phytoplankton cell derived from the actual population of cells that exhibit a certain size distribution. Because the size distribution is narrow the mean is meaningful in a sense that it represents an "*average*" cell within a population of similar cells.

Mean absorption efficiency factor $\overline{Q_a}$

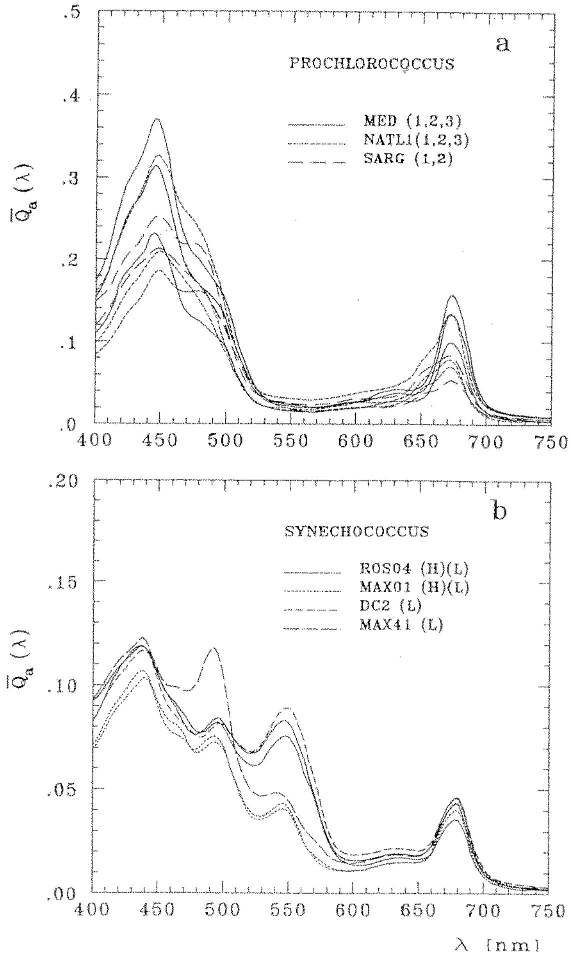

Size distribution $N(D)/V$

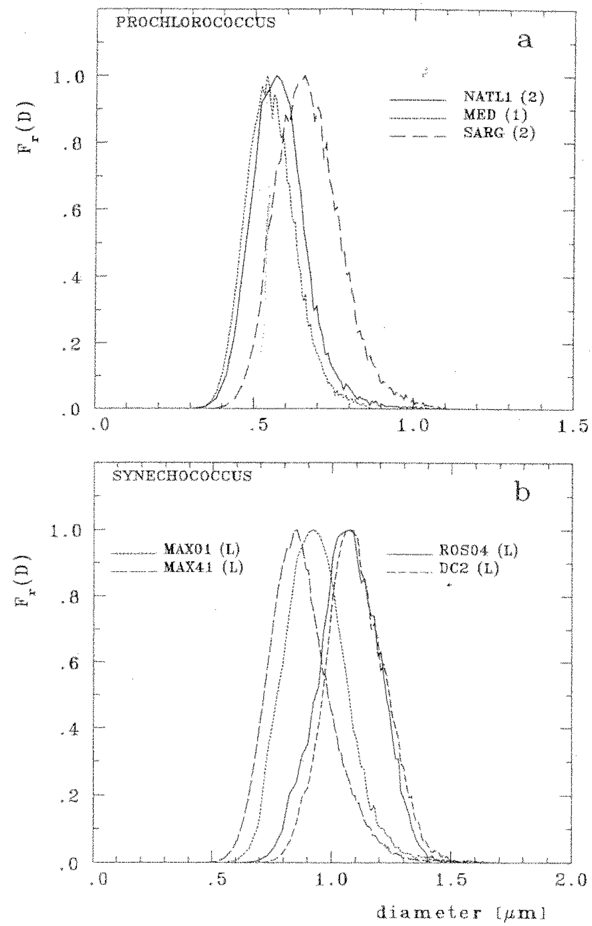

(Morel et al. 1993)

Comparison of experimental data of absorption efficiency for various phytoplankton and heterotrophic microorganisms with theoretical curve

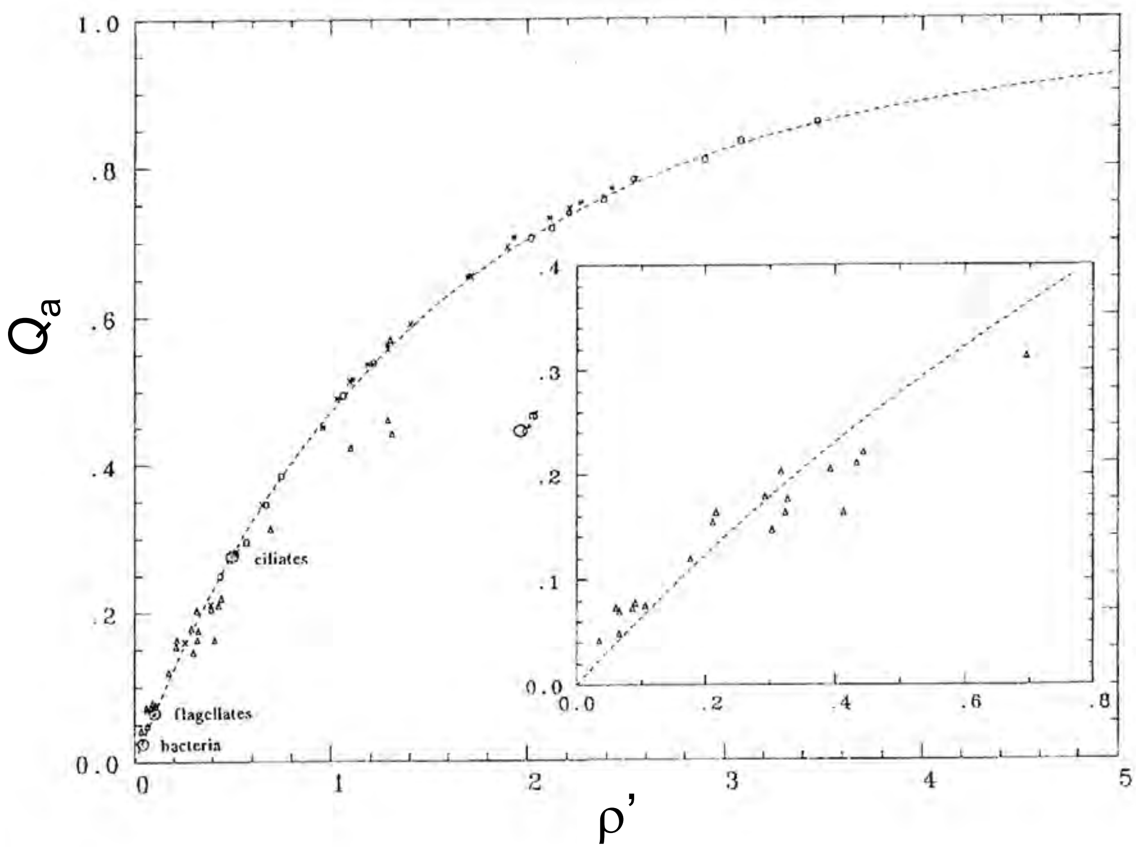

Figure 1. The theoretical variations of Q_a, the efficiency factor for absorption (dashed curves), as a function of the dimensionless parameter ρ',. The triangles are experimental determinations of Q_a (at 675 nm) for various algae (Morel and Bricaud, 1986; Ahn, 1990); other symbols are for determinations of 3 algal species studied by Sosik (1988). The values for heterotrophic organisms, as indicated, come from Morel and Ahn (1990, 1991). The inset is an enlargment of the initial part of the curve.

(Morel 1991)

Scattering efficiency factor for a single particle

$$Q_b(\lambda) = F_b(\lambda) / F_o(\lambda)$$

$F_o(\lambda)$ - spectral radiant power intercepted by geometrical cross-section of particle

$F_b(\lambda)$ - spectral radiant power scattered by particle in all directions

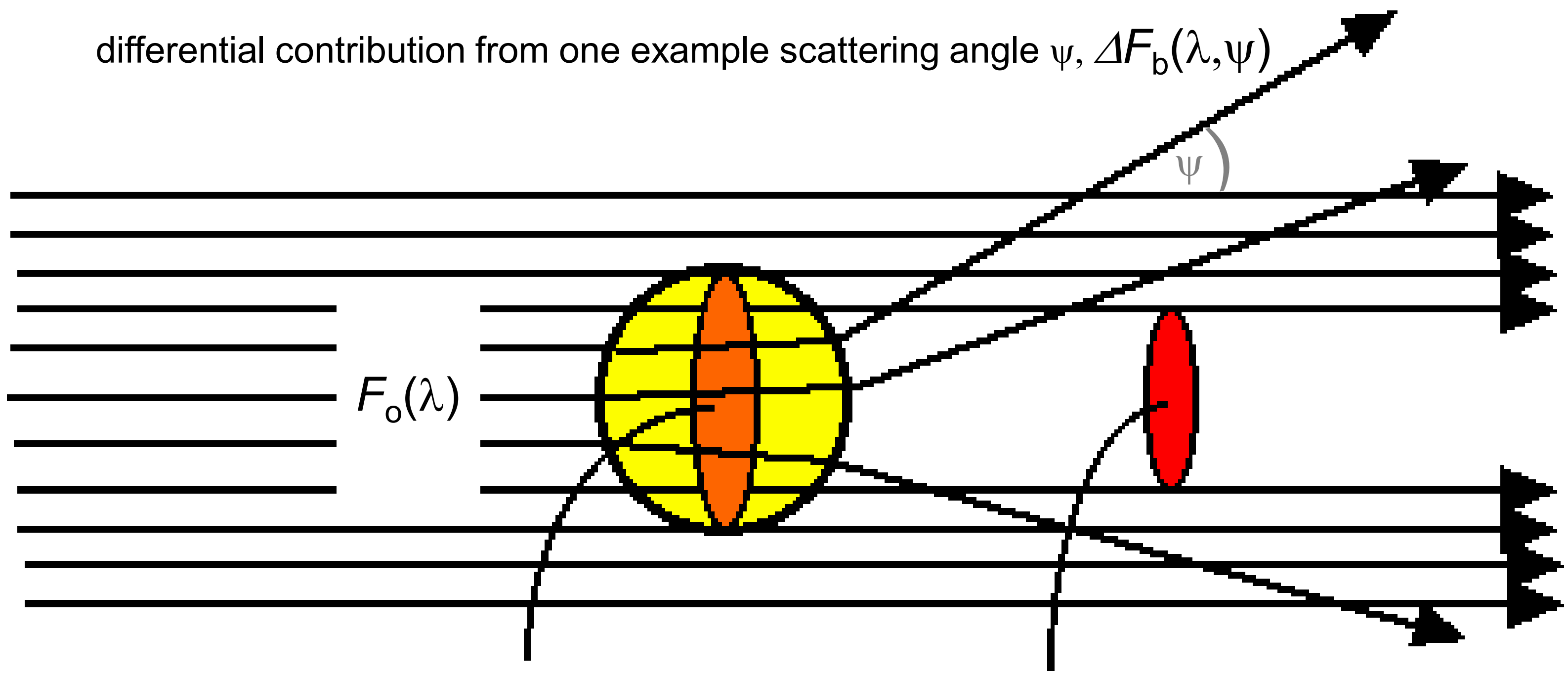

G

Geometrical cross-section

$\sigma_b(\lambda) = Q_b(\lambda)\, G$

Scattering cross-section

Note: ψ-dependent differential scattering efficiency and cross-section can also be defined

Theoretical dependence of optical efficiency factors on particle properties parameterized in terms of phase shift parameter ρ

$\rho = 2\,\alpha\,(n - 1)$ where n is the refractive index of particle relative to water

Absorption efficiency	Scattering efficiency	Attenuation efficiency		
$Q_a = F_a/F_o$	$Q_b = F_b/F_o$	$Q_c = F_c/F_o$	$F_c = F_a + F_b$	$Q_c = Q_a + Q_b$

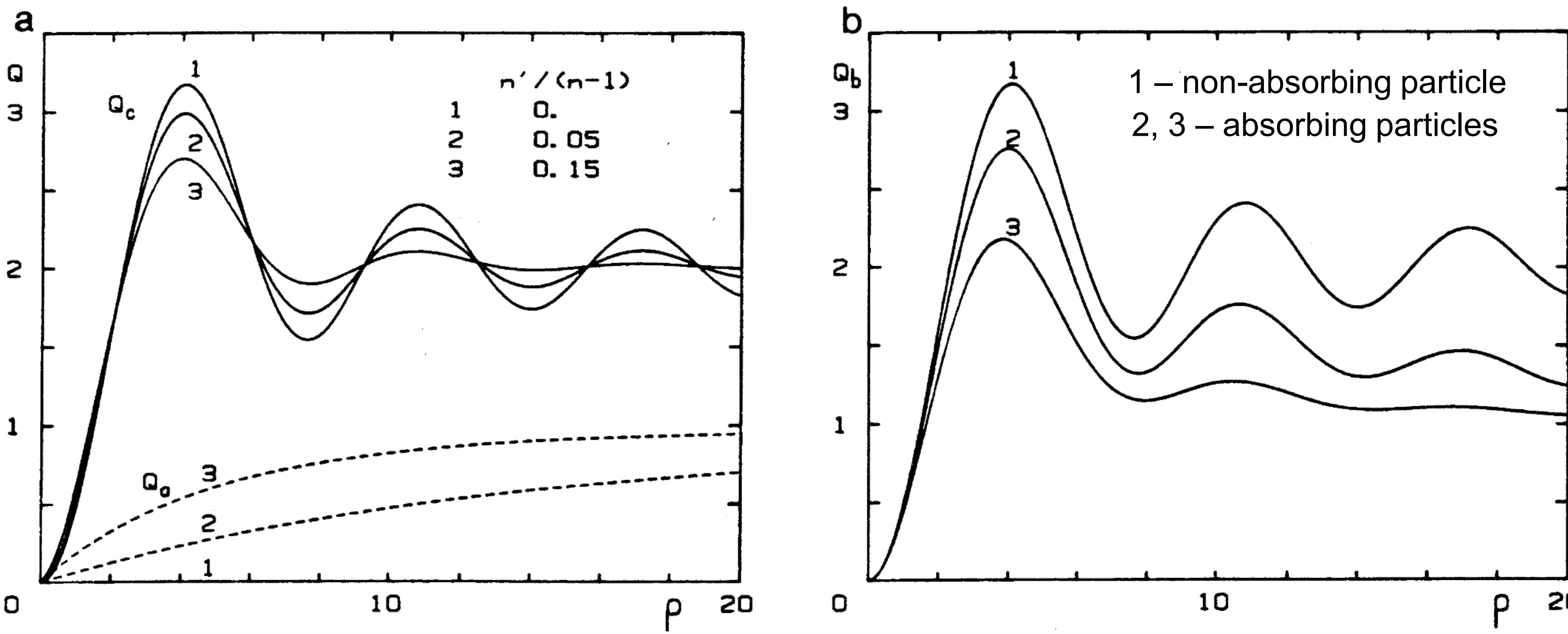

FIG. 3. Variations of the efficiency factors for attenuation, Q_c, *for absorption*, Q_a (a), and for scattering, Q_b (b) vs. the parameter $\varrho = 2\,\alpha(n-1)$, for increasing values of the ratio $n'/(n-1)$ where n and n' are the real and imaginary parts of the relative refractive index of the particles.

(Morel and Bricaud 1986)

The effect of polydispersion on attenuation efficiency

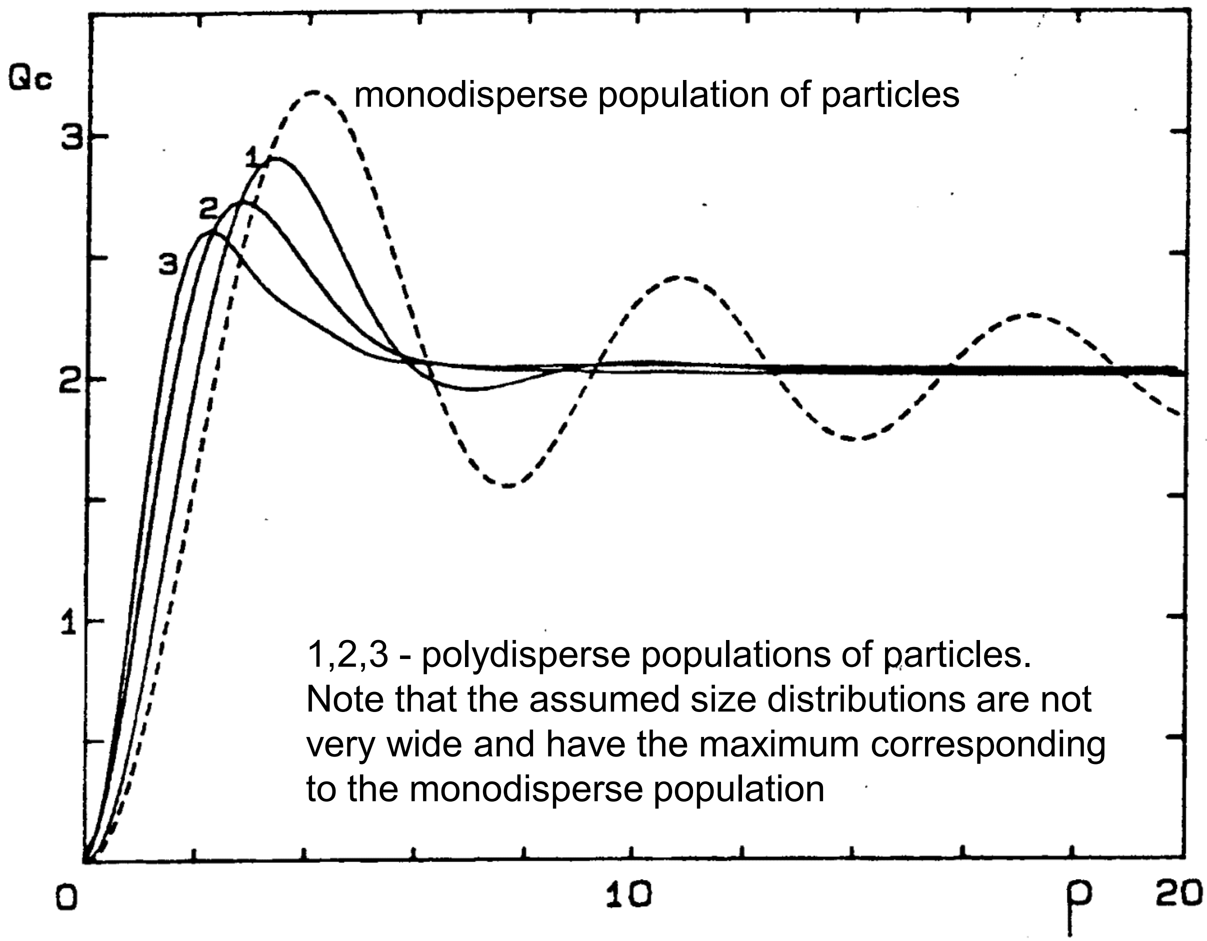

FIG. 4. Mean efficiency factor for attenuation Q_c of a "mean" particle representative of a polydispersed population, plotted as a function of ϱ_m, *the* ϱ value which corresponds to the maximum of the size distribution function $F(\varrho)$ (see Equation 17). The index of refraction is real (no absorption) and the curves 1 and 3 correspond to log-normal distributions such as $F(\varrho_M/2) = F(2\varrho_M)$ = respectively 0.01, 0.1, 0.3 $F(\varrho_M)$. The dashed curve, redrawn from Fig. 3 for $n' = 0$, represents the limiting case of a population of monosized particles.

(Morel and Bricaud 1986)

Comparison of experimental data of scattering efficiency for various phytoplankton and heterotrophic microorganisms with theoretical curves

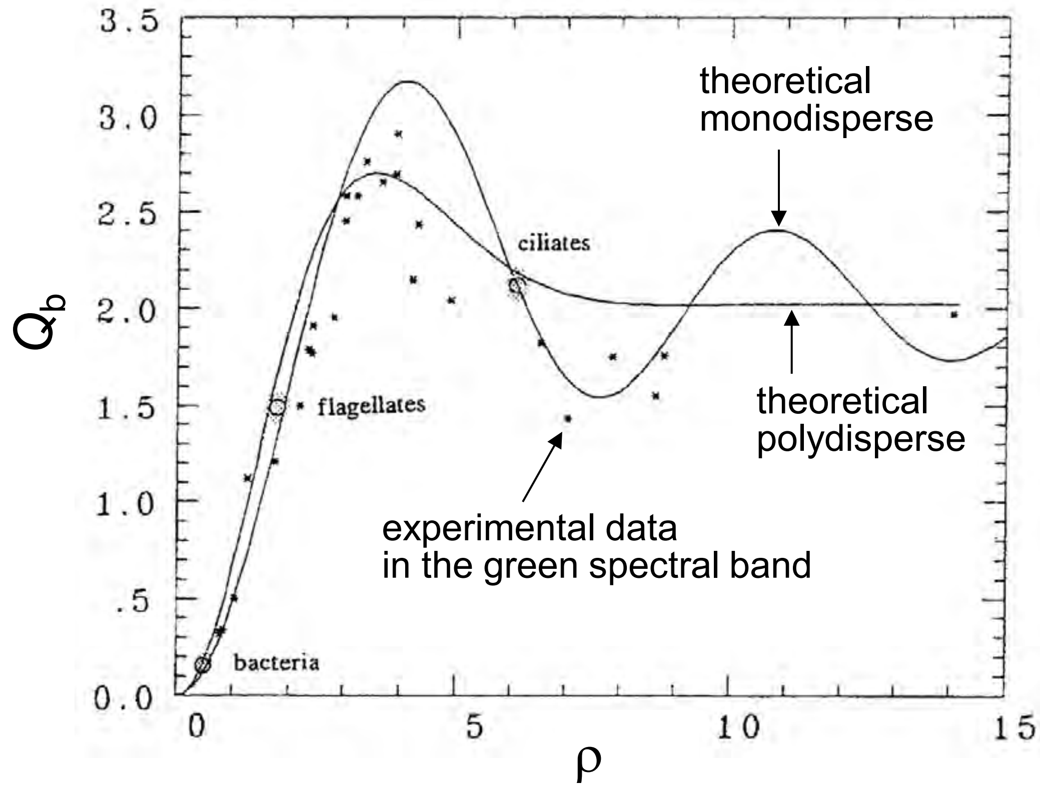

Figure 2. The theoretical variations of Q_b, the efficiency factor for scattering by non absorbing spheres (solid curve with marked oscillations) as a function of the dimensionless parameter ρ. The smoothed curve is for an averaged $\bar{Q}_b$ to be applied for population with a log - normal size distribution. The crosses are the $\bar{Q}_b$ values (at $\lambda \sim 580$ nm) determined for various phytoplankters grown in culture (see Table 1 in Morel and Bricaud, 1986); additional data for algal cells come from Ahn (1990). The circles indicate the $\bar{Q}_b$ values (at $\lambda \sim 550$ nm) determined for free living marine bacteria, heterotrophic flagellates, and naked ciliates, (Morel and Ahn, 1990; 1991).

(Morel 1991)

Spectra of scattering efficiency for various phototrophic and heterotrophic microorganisms derived from measurements

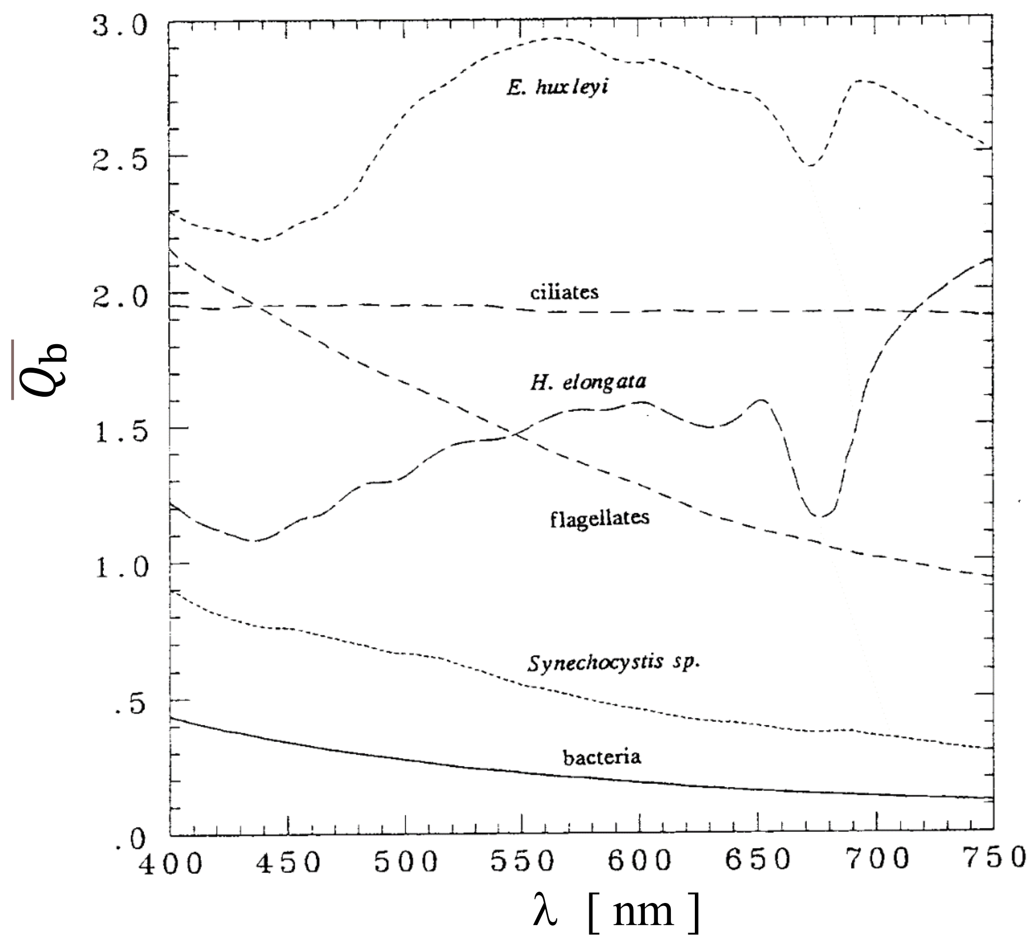

Note: Ciliates are the largest particles (~30 μm) in this comparison

Note: Bacteria are the smallest particles (~0.5 μm)

Figure 3. Spectral variations of Q_b within the 400-750 nm range of various phototrophic and heterotrophic organisms as experimentally determined (Morel and Ahn, 1990, 1991).

(Morel 1991)

D = 3.4 μm
n = 1.07

for visible light:

α = 20 – 35

ρ = 3 – 5

Optical efficiency factors Q_c, Q_b, and Q_a :

Examples for monospecific cultures of phytoplankton cells
(derived from laboratory measurements of absorption and attenuation coefficients, and size distribution made on cultures)

D = 1.2 μm
n = 1.0325

for visible light:

α = 7 – 13

ρ = 0.5 – 1.5

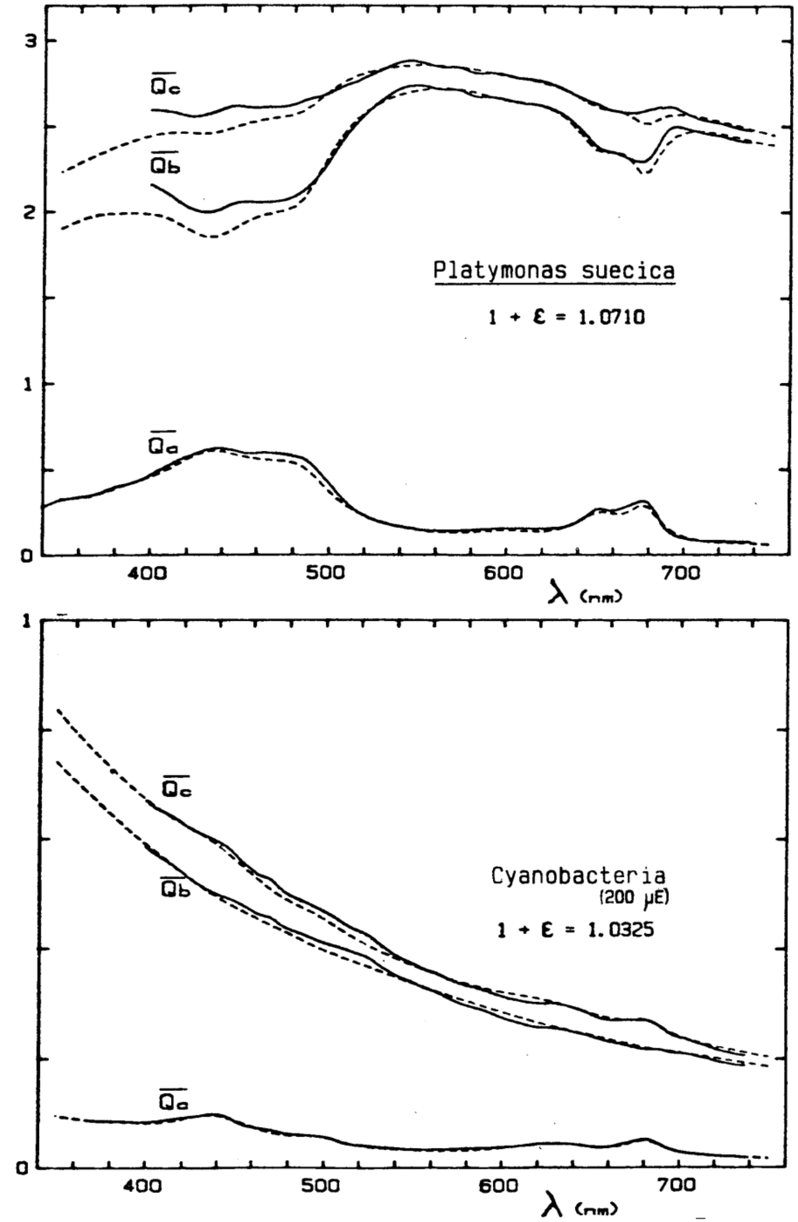

FIG. 14. Spectral variations of the mean efficiency factors for attenuation ($\bar{Q}_c$), scattering ($\bar{Q}_b$) and absorption ($\bar{Q}_a$), deduced from the attenuation and absorption coefficients experimentally determined (continuous lines), for two phytoplanktonic species. The variations of $\bar{Q}_c$, $\bar{Q}_b$ and $\bar{Q}_a$ obtained from a theoretical model (see text) are shown as dashed lines. The central value of the real part of the refractive index, $1 + \epsilon$, leading to the best theory/experiment agreement is indicated on the Figures.

(Morel and Bricaud 1986)

Scattering phase function: Effects of particle size and refractive index

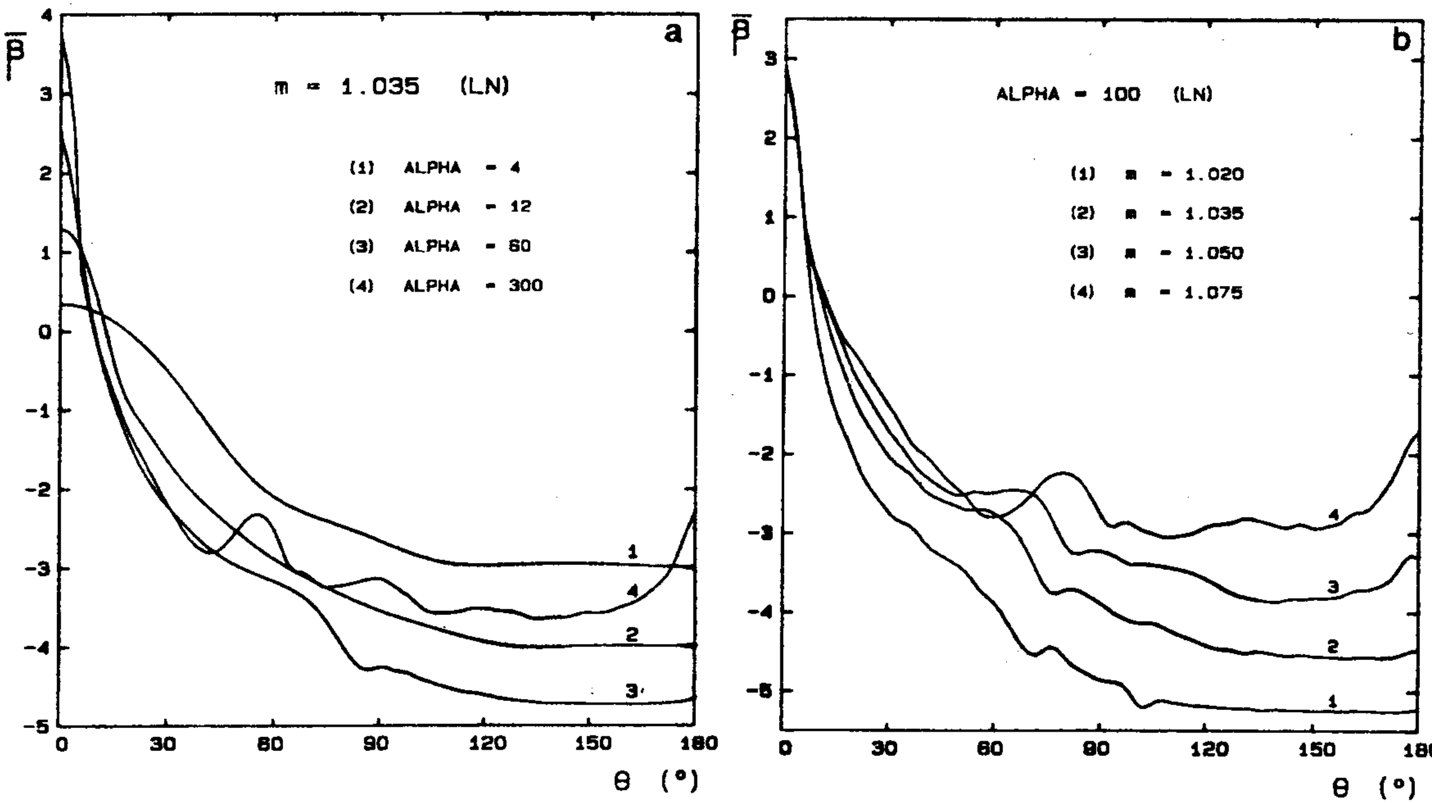

FIG. 6. (a) Normalized volume scattering function $\bar{\beta}(\theta)$ for increasing α_M values (increasing size) and for $m = 1.035$. (b) Normalized volume scattering function $\bar{\beta}(\theta)$ for increasing (real) index of refraction and for $\alpha_M = 100$. For Fig. 6a and b the log normal size distribution used is as in Fig. 5. The "bump" which occurs at about 75° for $m = 1.075$ and at smaller angles when the refractive index decreases (see also Fig. 6a) is the first "rainbow", at 138° for water droplets ($n = 1.33$). It appears for sufficiently large and perfect spheres. Thus it is unlikely that it can be observed for algal cells.

(Morel and Bricaud 1986)

Normalized scattering function for various microorganisms (from Mie calculations)

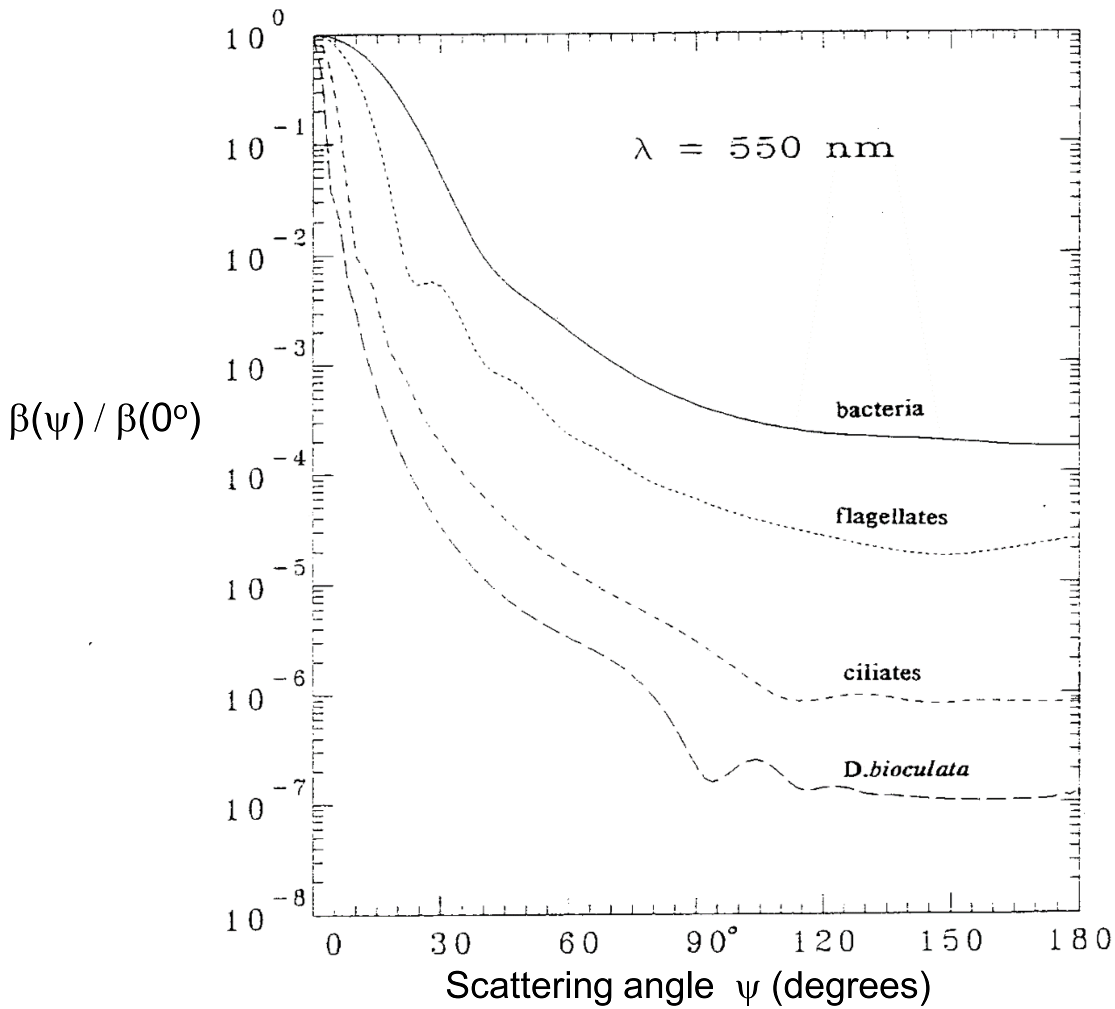

Figure 6. Volume scattering function (normalized at $\theta = 0°$ and for $\lambda = 550$ nm) computed for various organisms by using their refractive index and size distribution as experimentally determined (see text).

(Morel 1991)

Backscattering ratio versus particle size parameter

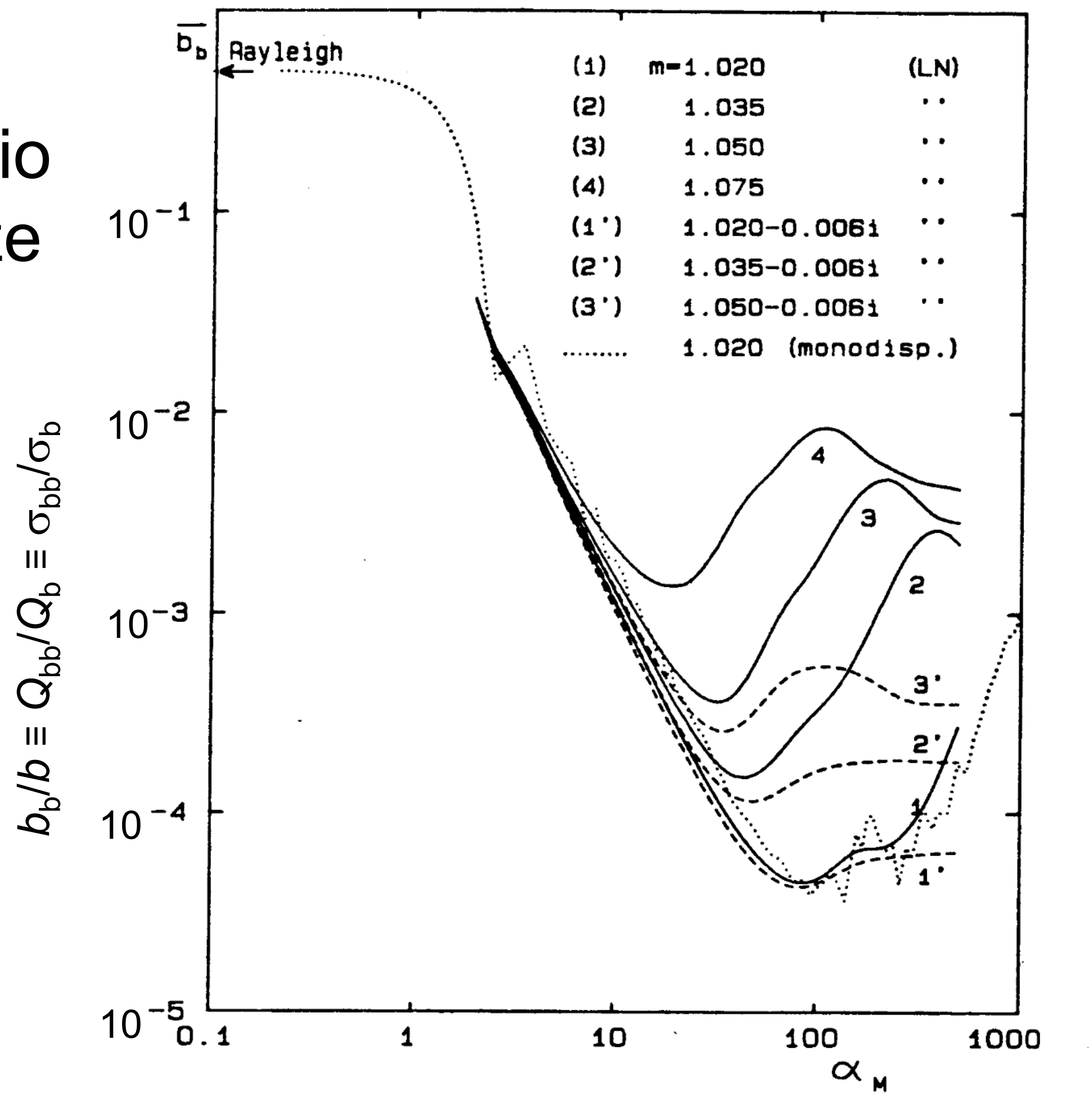

FIG. 8. Variations of the backscattering ratio $\bar{b}_b$ ($= b_b/b$) vs. the modal relative size α_M (same log-normal law as before in Fig. 5). The different curves correspond to various values of the refractive index given in inset. The curve for a monodispersed population (with $m = 1.02$) is also shown (dotted line). The arrow indicates the limiting value of b_b/b ($=0.5$) when α tends toward 0 (Rayleigh domain).

(Morel and Bricaud 1986)

INTERSPECIES OPTICAL VARIABILITY OF PLANKTON MICROORGANISMS

Particle size and complex refractive index are the first-order determinants of interspecies variability of single-particle optical properties

Plankton microorganisms

Table 1. Microbial components in the database and source of raw data. Values for the average equivalent spherical diameter (D), the real part of refractive index at 550 nm (n), and imaginary part of refractive index at 440 and 675 nm (n') are also given for each component.

i	Label	Microbial species	D [μm]	n 550 nm	$n' \cdot 10^3$ 440 nm	$n' \cdot 10^3$ 675 nm	Source of raw data
1	VIRU	Viruses	0.07	1.050	0	0	Stramski and Kiefer, 1991
2	HBAC	Heterotrophic bacteria	0.55	1.055	0.509	0.057	Stramski and Kiefer, 1990
3	PROC	generic Prochlorophyte; the average of:	0.66	1.051	18.51	10.30	
		PMED - Prochlorococcus strain MED	0.59	1.055	23.25	13.77	Morel et al., 1993
		PNAS - average of Prochlorococcus strains NATL and SARG	0.70	1.046	13.78	6.687	Morel et al., 1993
4	SYNE	generic Synechococcus; the average of:	1.05	1.051	5.587	2.930	
		SM41 - Synechococcus strain MAX41 (Cyanophyceae)	0.92	1.047	5.415	2.905	Morel et al., 1993
		SM01 - Synechococcus strain MAX01 (Cyanophyceae)	0.94	1.049	4.505	2.547	Morel et al., 1993
		SROS - Synechococcus strain ROS04 (Cyanophyceae)	1.08	1.049	4.516	2.154	Morel et al., 1993
		SDC2 - Synechococcus strain DC2 (Cyanophyceae)	1.14	1.050	4.249	2.375	Morel et al., 1993
		S103 - Synechococcus strain WH8103 (Cyanophyceae)	1.14	1.062	9.251	4.668	Stramski et al., 1995
5	SYMA	generic phycocyanin-rich picophytoplankton; the average of:	1.41	1.055	6.495	2.757	
		SCYS - Synechocystis (Cyanophyceae)	1.39	1.050	4.530	1.910	Ahn et al., 1992
		MARI - Anacystis marina (Cyanophyceae)	1.43	1.060	8.460	3.603	Ahn et al., 1992
6	PING	Pavlova pinguis (Haptophyceae)	3.97	1.046	4.177	2.709	Bricaud et al., 1988
7	PSEU	Thalassiosira pseudonana (Bacillariophyceae)	3.99	1.045	9.231	7.397	Stramski and Reynolds, 1993
8	LUTH	Pavlova lutheri (Haptophyceae)	4.26	1.045	5.767	2.403	Bricaud et al., 1988
9	GALB	Isochrysis galbana (Haptophyceae)	4.45	1.056	7.673	5.101	Ahn et al., 1992
10	HUXL	Emiliania huxleyi (Haptophyceae)	4.93	1.050	5.012	2.950	Ahn et al., 1992
11	CRUE	Porphyridium cruentum (Rhodophyceae)	5.22	1.051	3.351	2.443	Bricaud et al., 1988
12	FRAG	Chroomonas fragarioides (Cryptophyceae)	5.57	1.039	4.275	2.904	Ahn et al., 1993
13	PARV	Prymnesium parvum (Haptophyceae)	6.41	1.045	2.158	1.329	Bricaud et al., 1988
14	BIOC	Dunaliella bioculata (Chlorophyceae)	6.71	1.038	10.49	7.839	Ahn et al., 1993
15	TERT	Dunaliella tertiolecta (Chlorophyceae)	7.59	1.063	6.260	5.076	Stramski et al., 1993
16	CURV	Chaetoceros curvisetum (Bacillariophyceae)	7.73	1.024	2.877	1.480	Bricaud et al., 1988
17	ELON	Hymenomonas elongata (Haptophyceae)	11.77	1.046	13.87	7.591	Ahn et al., 1992
18	MICA	Prorocentrum micans (Dinophyceae)	27.64	1.045	2.466	1.710	Ahn et al., 1992

(Stramski et al. 2001)

Interspecies variability of absorption properties

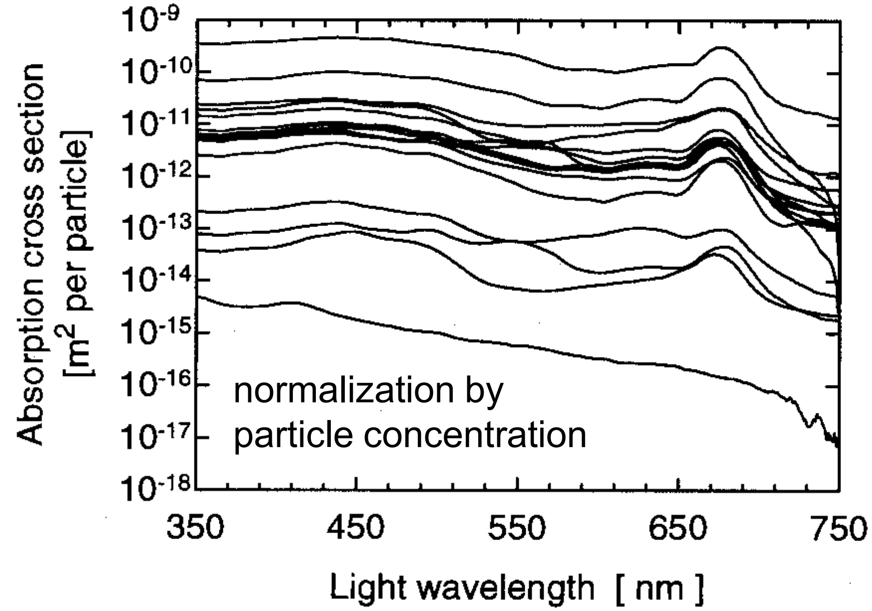

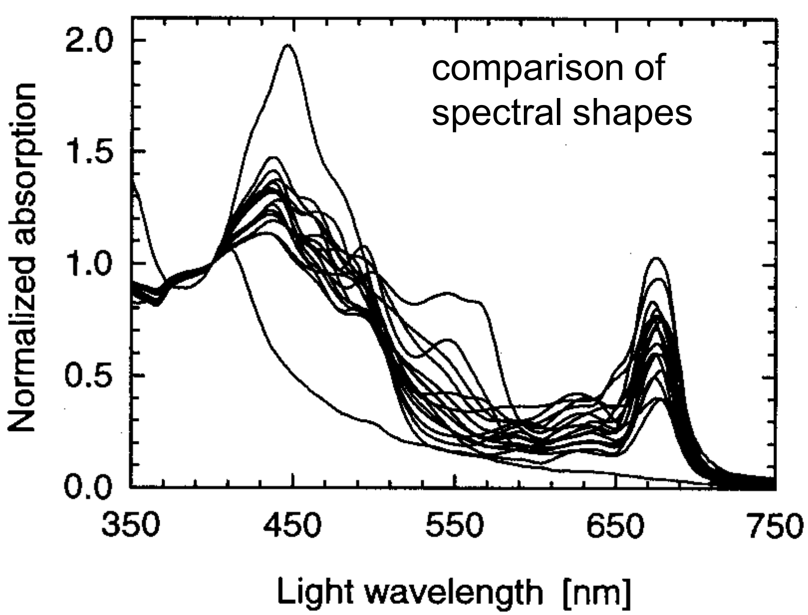

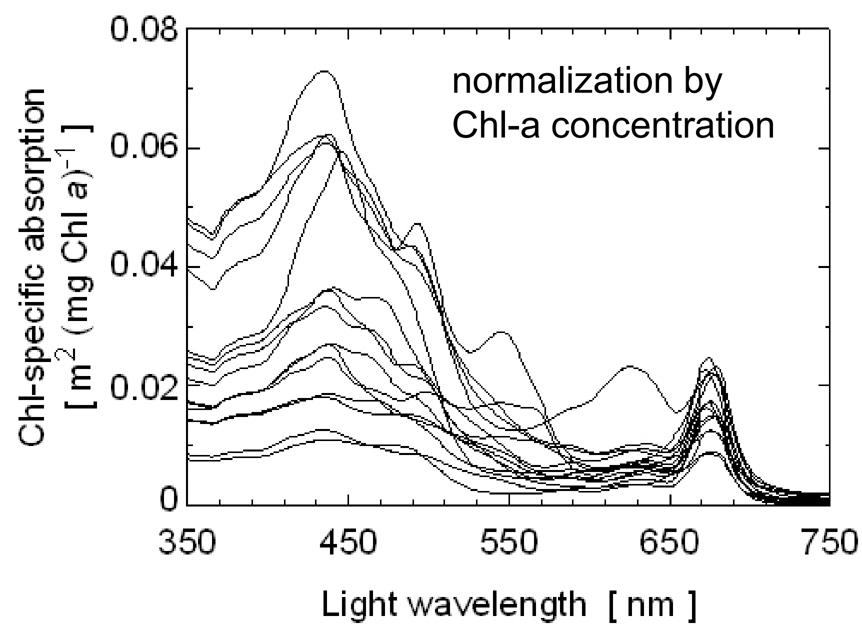

(Stramski et al. 2001)

Interspecies variability of scattering properties

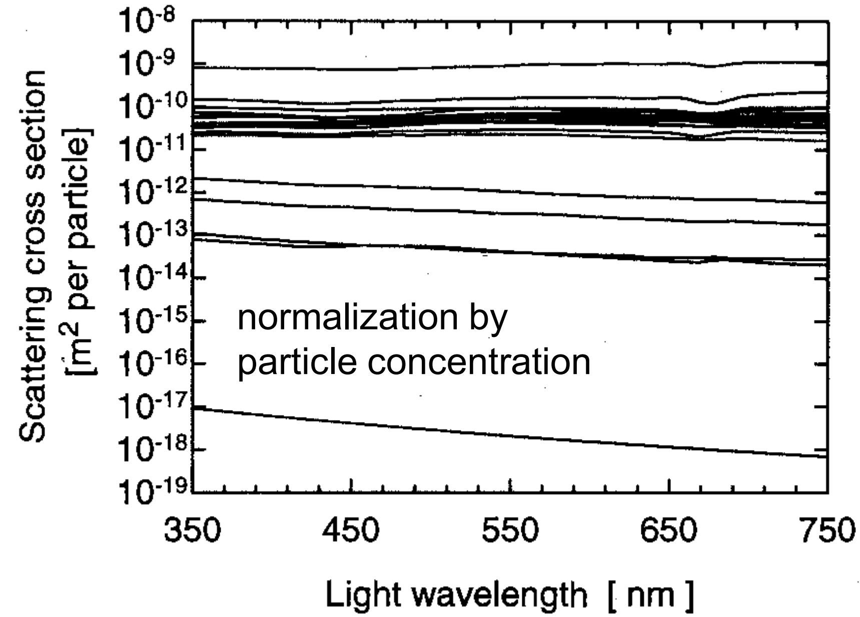

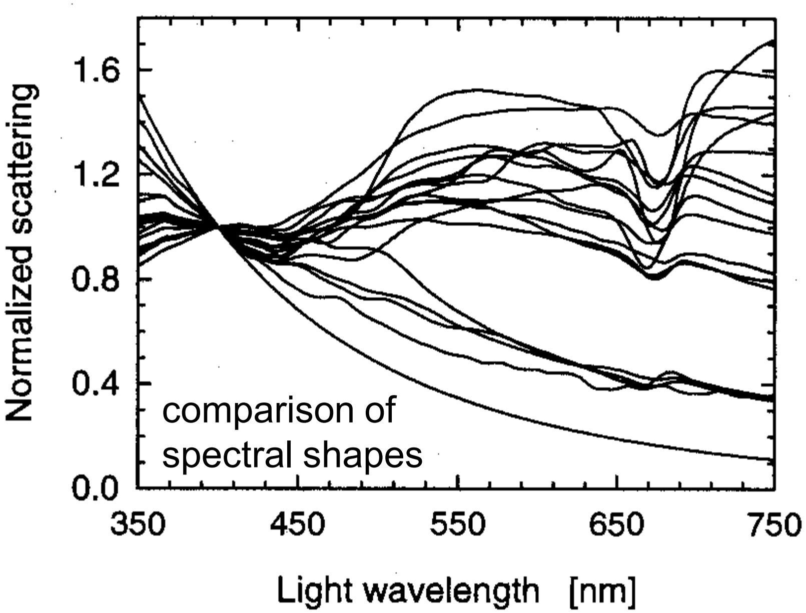

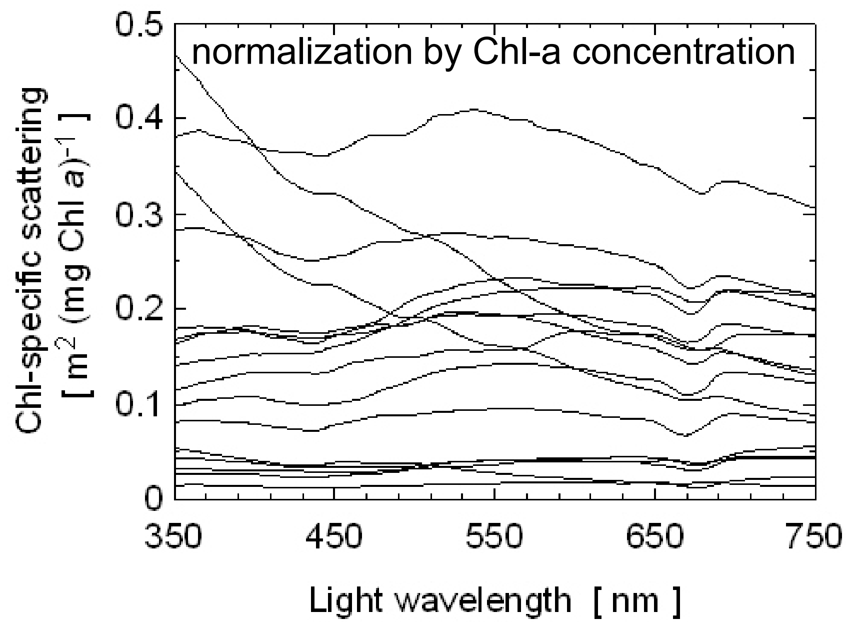

(Stramski et al. 2001)

INTRASPECIES OPTICAL VARIABILITY OF PLANKTON MICROORGANISMS

Plankton optical properties vary in response to varying growth conditions:
light, nutrients, temperature

Intraspecies variability due to acclimation to growth irradiance
cyanobacteria *Synechocystis*

Absorption | Scattering

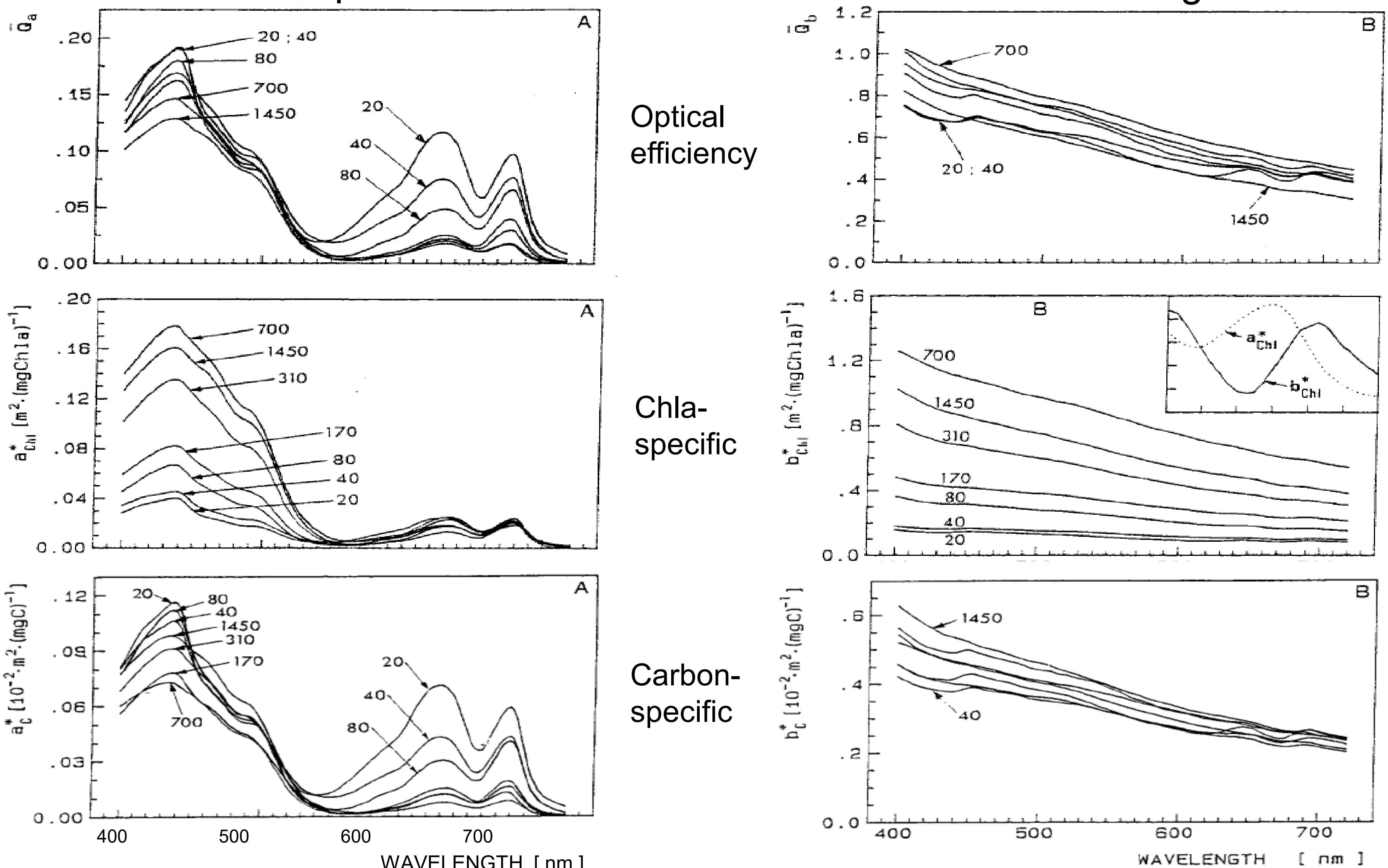

(Stramski and Morel 1990)

Intraspecies variability over a diel cycle

diatom *Thalassiosira pseudonana*

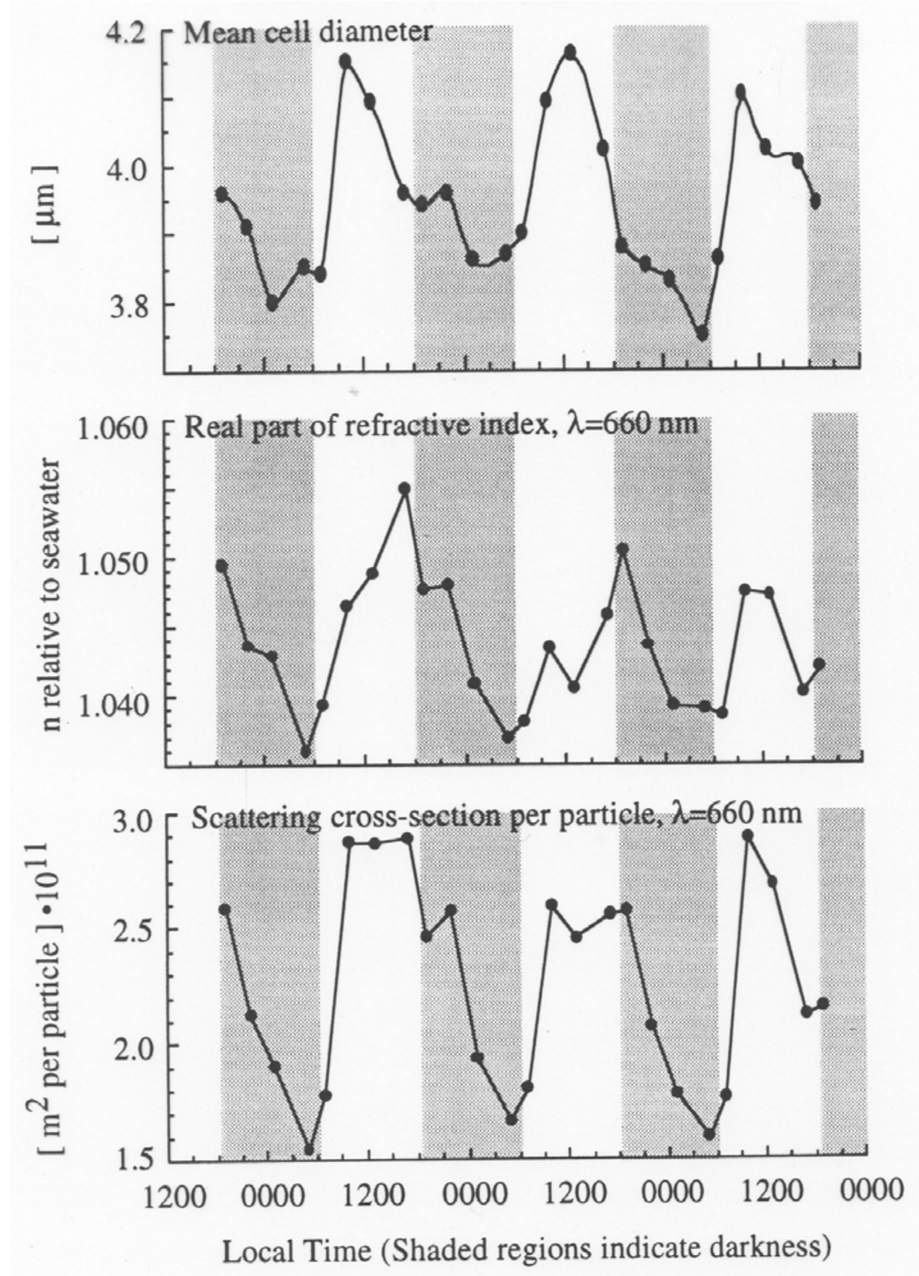

(Stramski and Reynolds 1993)

Optical properties of heterotrophic bacteria

Absorption

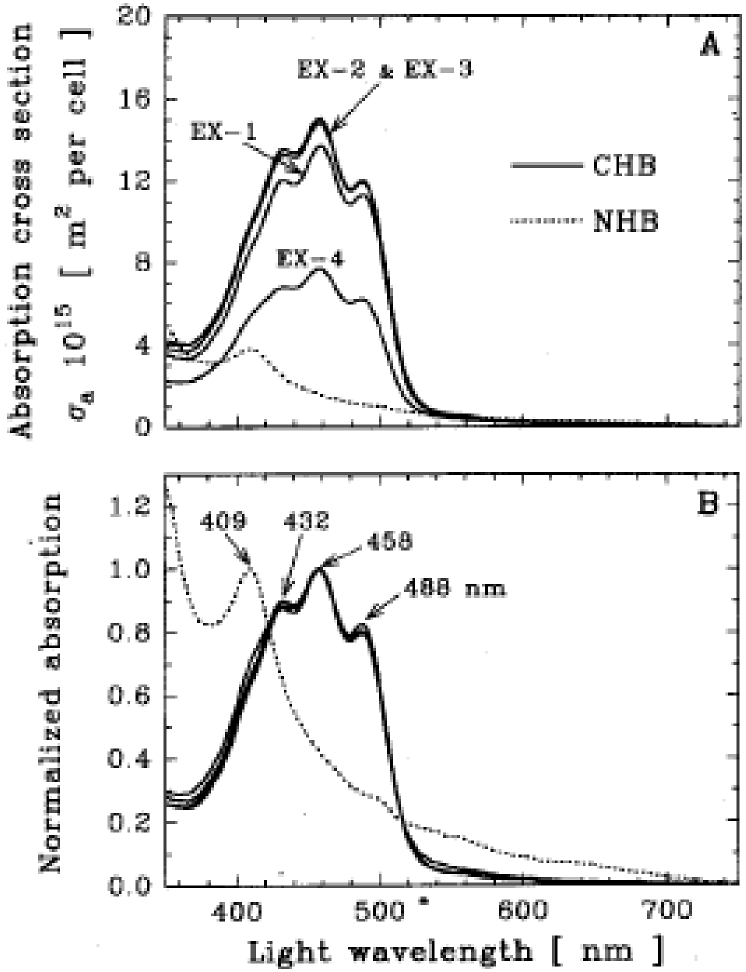

Beam attenuation

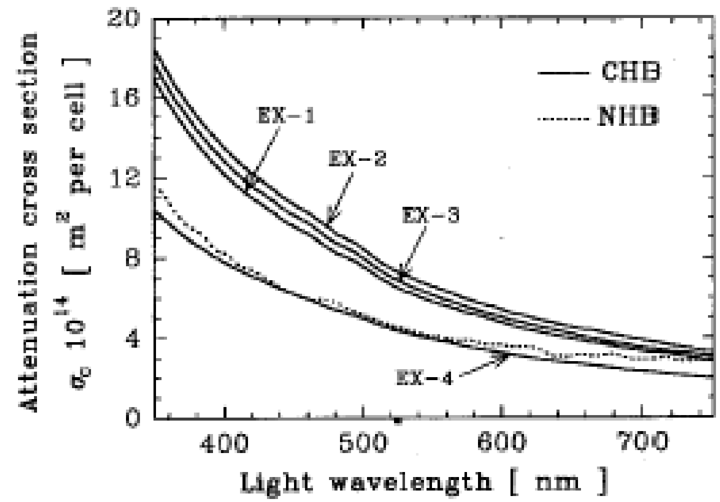

CHB Carotenoid-rich bacteria:
grown in nutrient-enriched seawater [EX-1 (light-dark cycle), EX-2 and EX-3 (dark)], and in nutrient-poor seawater (EX-4)

NHB Non-pigmented bacteria:
fast-growing in the absorption experiment and starved in the attenuation experiment

(Stramski and Kiefer 1998)

Optical properties of mineral-rich particulate matter

Sample ID	Description	Origin
ILL_1	illite	Source Clay Minerals Repository, University of Missouri (ref. IMt-1)
ILL_2	as above but different PSD	as above
KAO_1	kaolinite (poorly crystallized)	as above (ref. KGa-2)
KAO_2	as above but different PSD	as above
MON_1	Ca-montmorillonite	as above (ref. SAz-1)
MON_2	as above but different PSD	as above
CAL_1	calcite	natural crystal
CAL_2	as above but different PSD	as above
QUA_1	quartz	natural crystal
SAH_1	atmospheric dust from Sahara	red rain event, Villefranche-sur-Mer, France
SAH_2	as above but different PSD	as above
AUS_1	surface soil dust	cliff shore, Palm Beach near Sydney, Australia
AUS_2	as above but different PSD	as above
ICE_1	ice-rafted particles	glacier runoff, Kongsfjord, Spitsbergen
ICE_2	as above but different PSD	as above
OAH_1	surface soil dust	Oahu, Hawaii Islands
OAH_2	as above but different PSD	as above
KUW_1	surface soil dust	Kuwait (eastern part, close to ocean)
KUW_2	as above but different PSD	as above
NIG_1	surface soil dust	southwest Nigeria
SAN_1	atmospheric dust	San Diego, California

(Stramski et al. 2007)

Mass-specific absorption

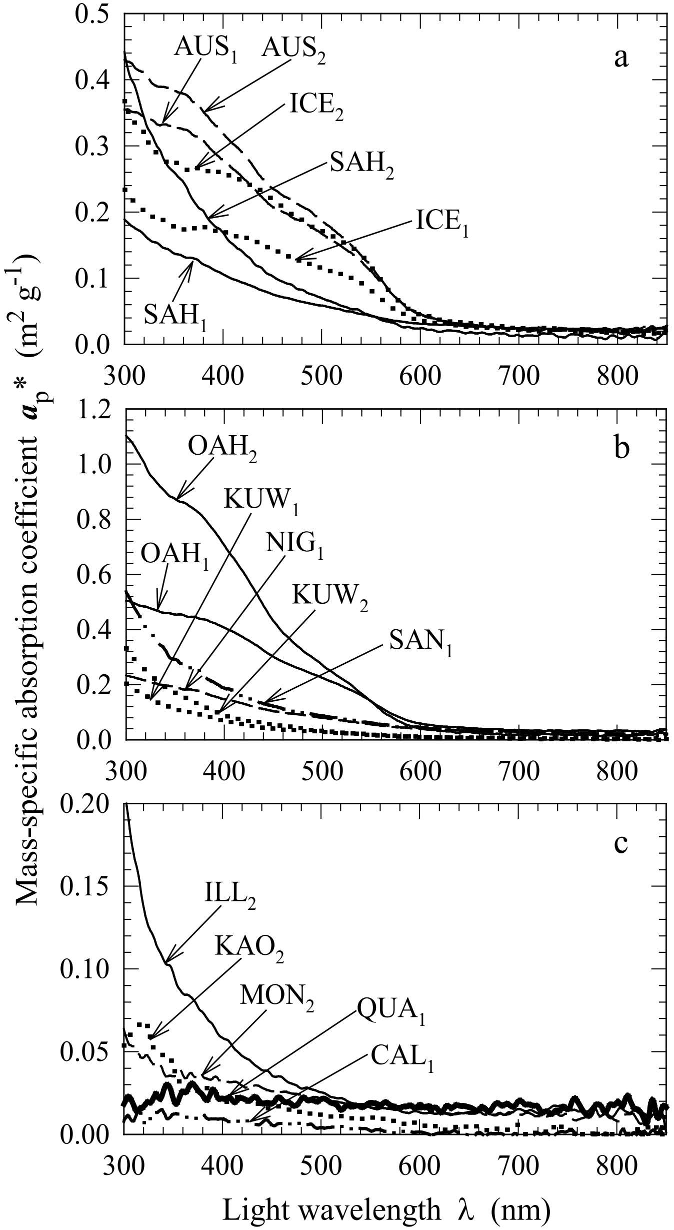

Mass-specific scattering

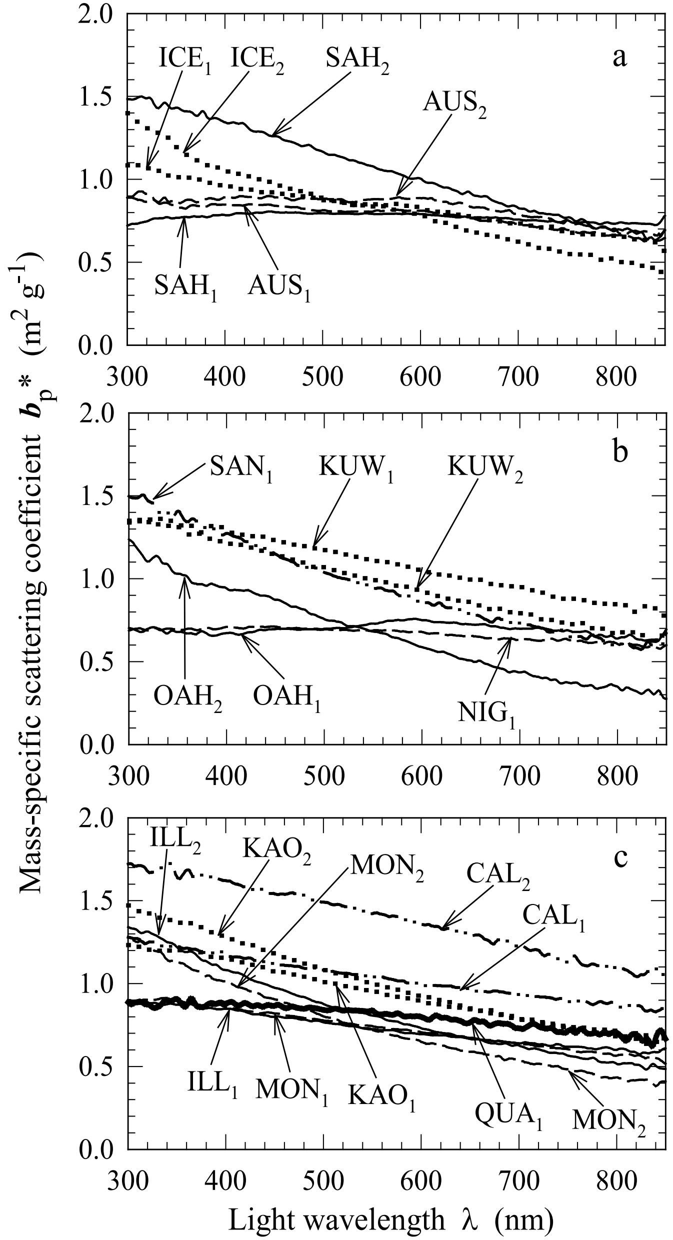

(Stramski et al. 2007)

(Babin and Stramski 2004)

Particle size distributions in the submicrometer range (TEM data < 0.2 μm)

Transmission electron microscopy (TEM)

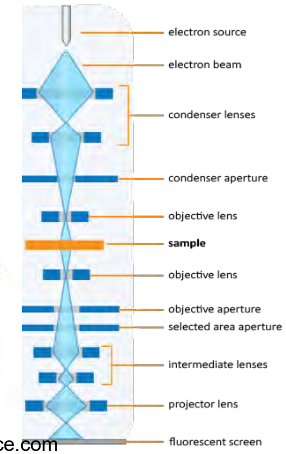

JEOL & nanoscience.com

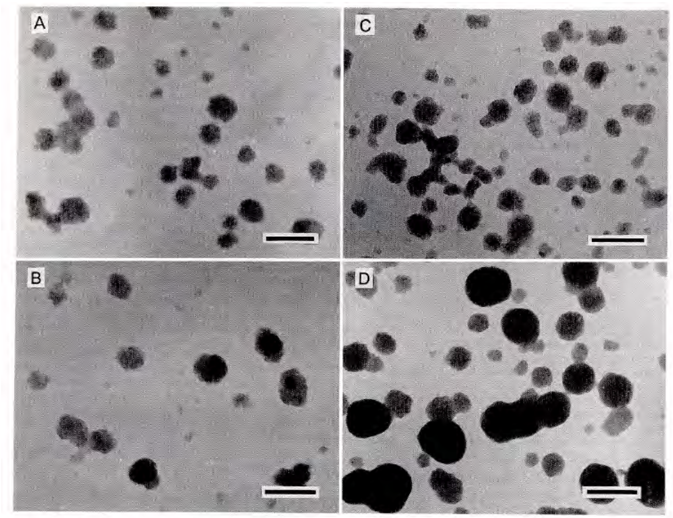

Fig. 3. TEM micrographs of small colloids: A—25-m depth, Scotian Shelf; B—300-m depth, Scotian slope; C—2,500-m depth, Sargasso Sea; D—30-m depth, open-water station in the Southern Ocean. Scale bars are 100 nm.

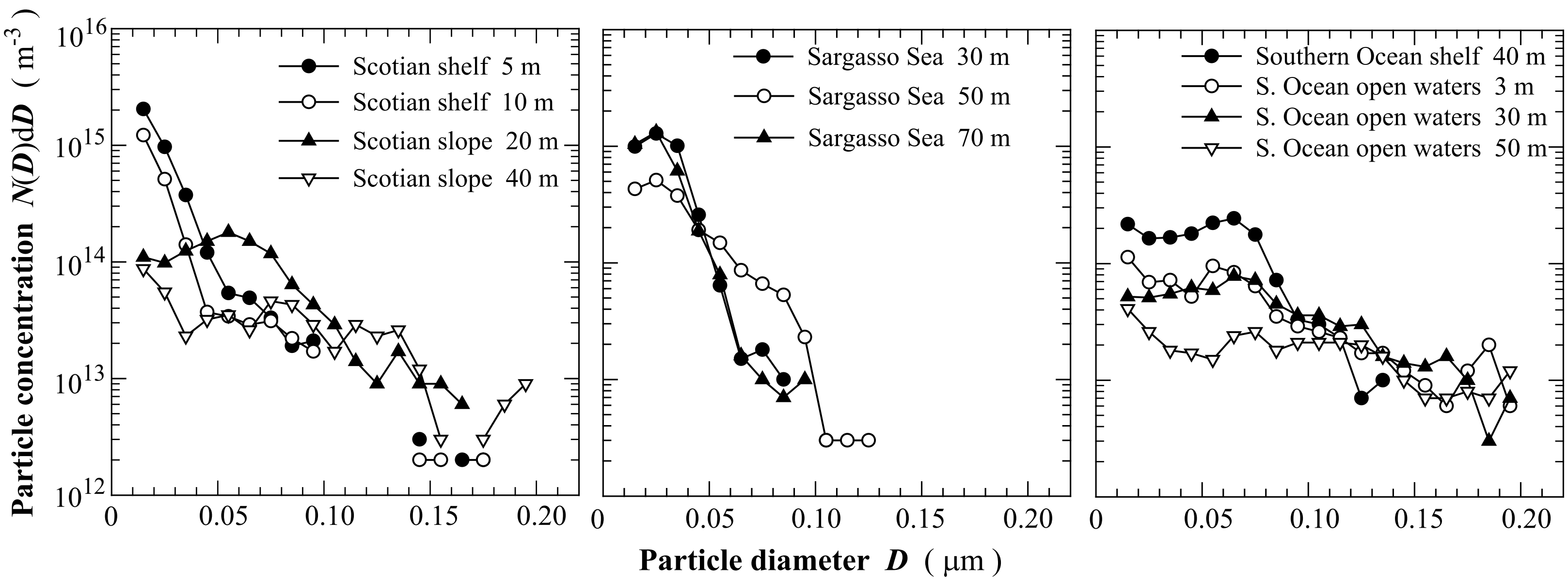

Wells and Goldberg (1994)

Particle size distributions in the submicrometer range (Coulter Counter data 0.4 – 1 μm)

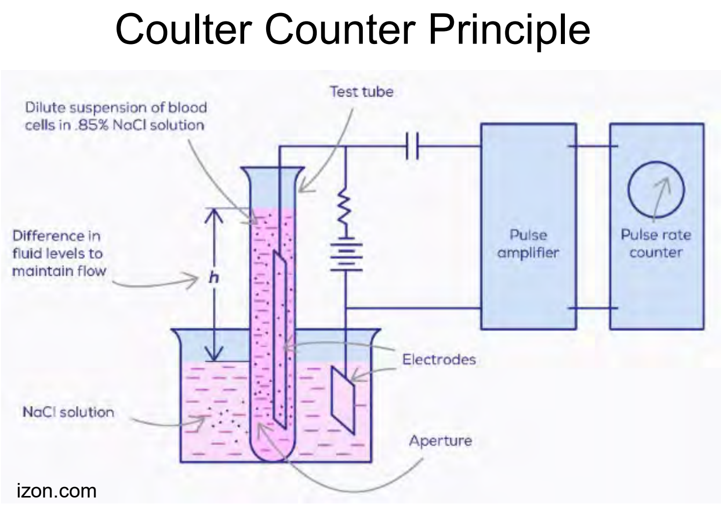

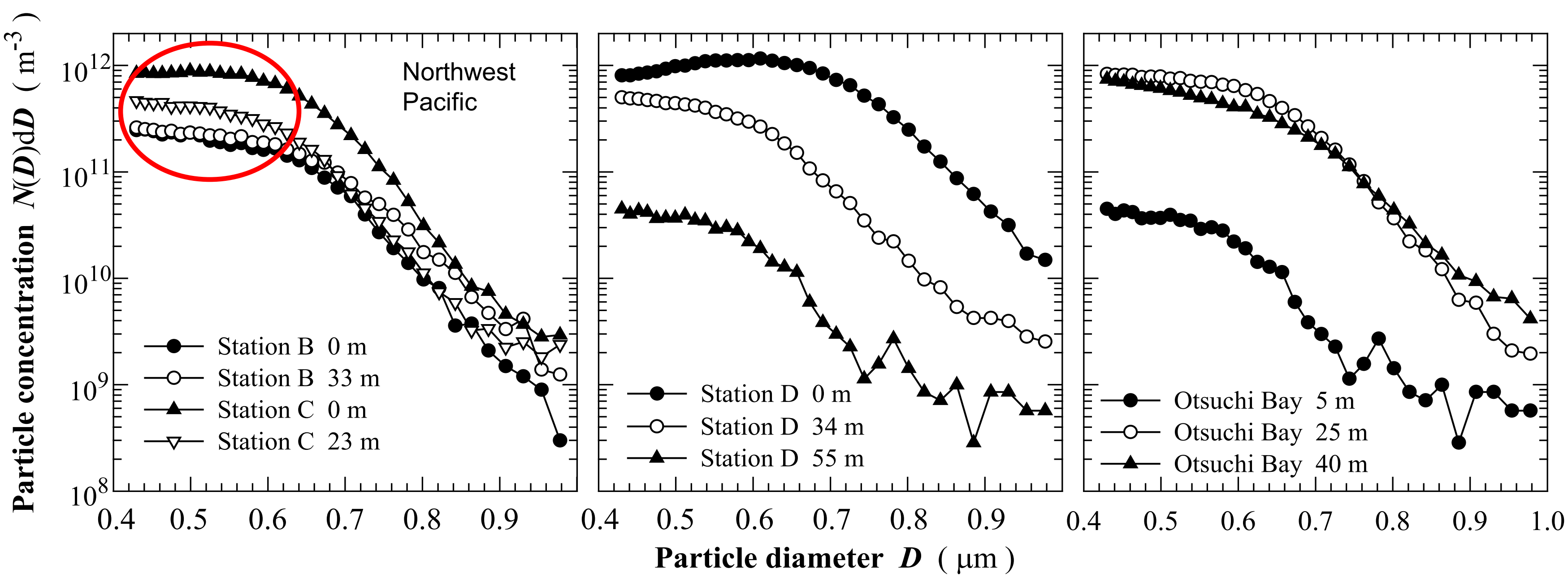

Yamasaki et al. (1998)

Assessment of scattering and backscattering coefficients of colloidal particles: Comparison with pure seawater

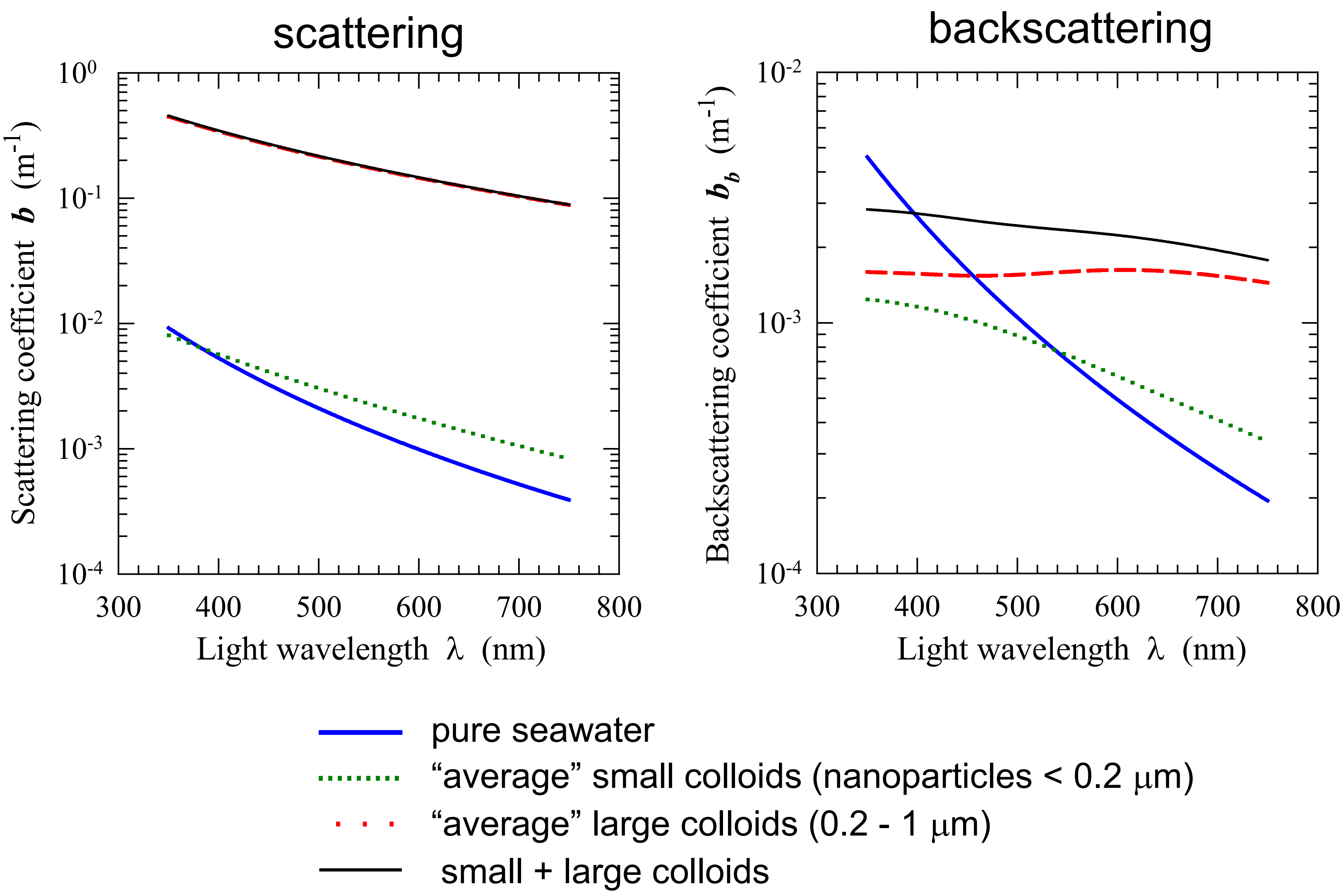

(Stramski and Woźniak 2005)

Nanoparticle Tracking Analysis (NTA)

- Nanoparticles illuminated by a beam of light
- Scattered-light images produced by individual nanoparticles are recorded over time
- Individual particle counting yields nanoparticle concentration
- Individual nanoparticle sizes are derived from determinations of mean squared displacement and Brownian diffusion coefficient (Stokes-Einstein equation)

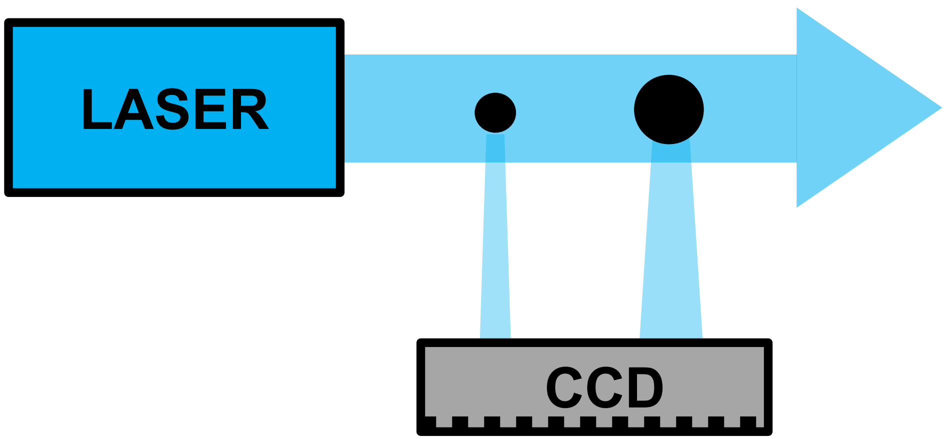

MANTA
Multispectral **A**dvanced
Nanoparticle **T**racking **A**nalysis

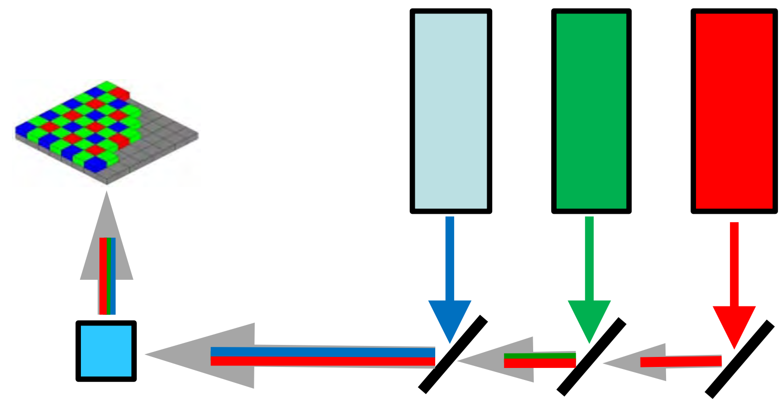

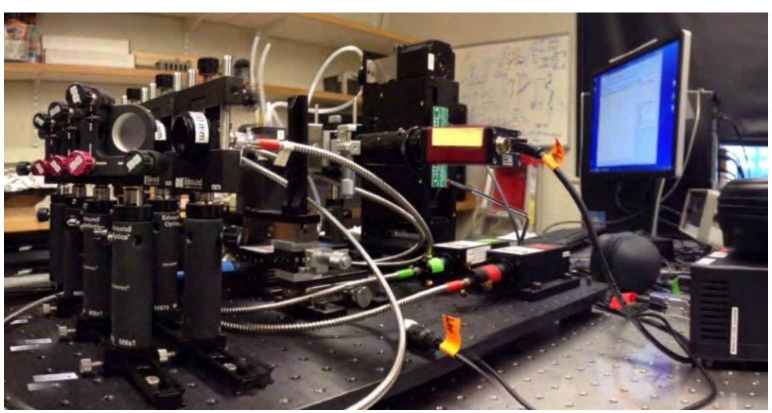

ViewSizer 3000

HORIBA Scientific

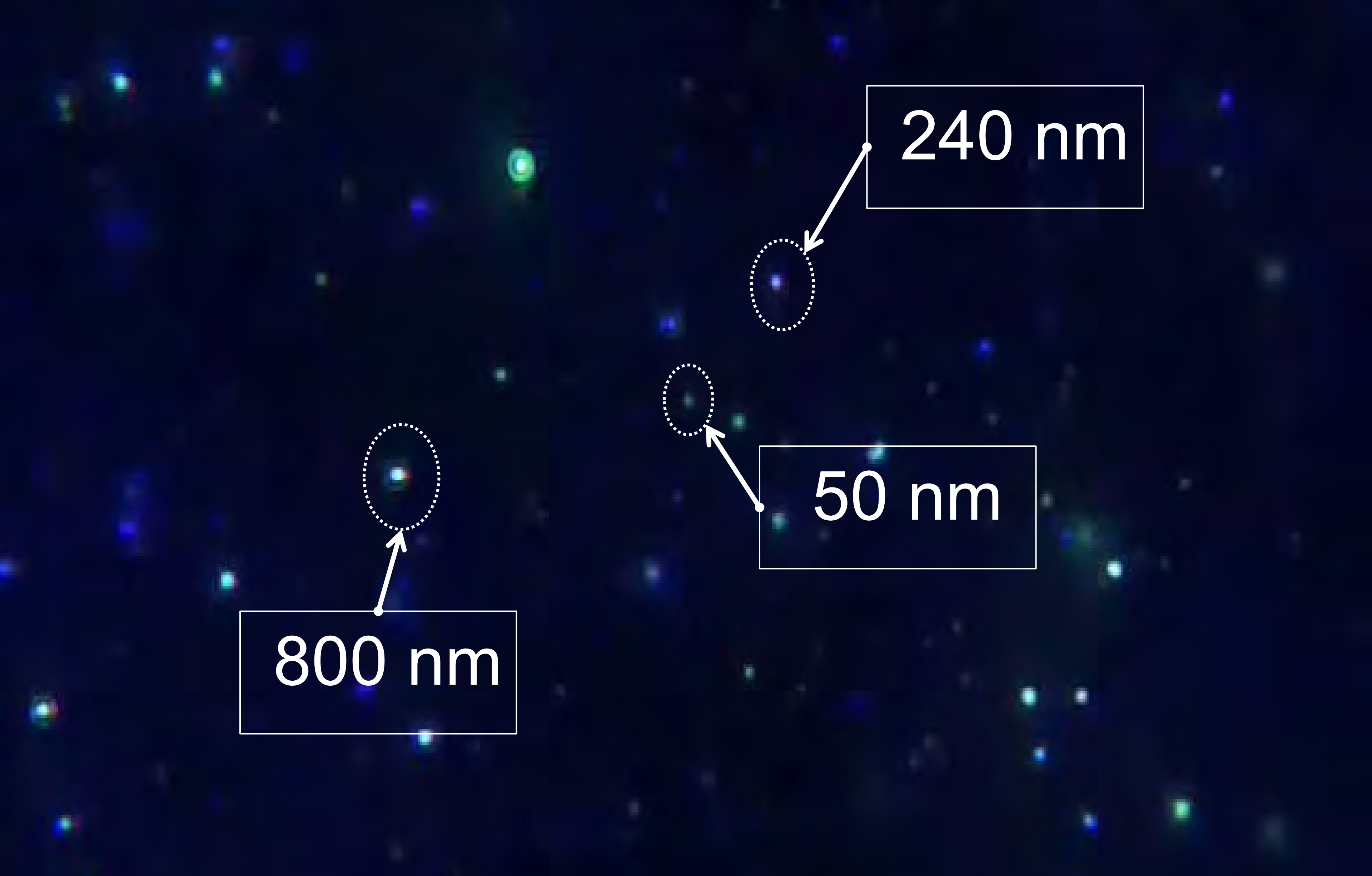

Measurement of a wide range of nanoparticle sizes simultaneously using novel MANTA technology (Multispectral Advanced Nanoparticle Tracking Analysis)

A superposition of 300 video frames acquired during 10 seconds illustrating trajectories of individual nanoparticles through time

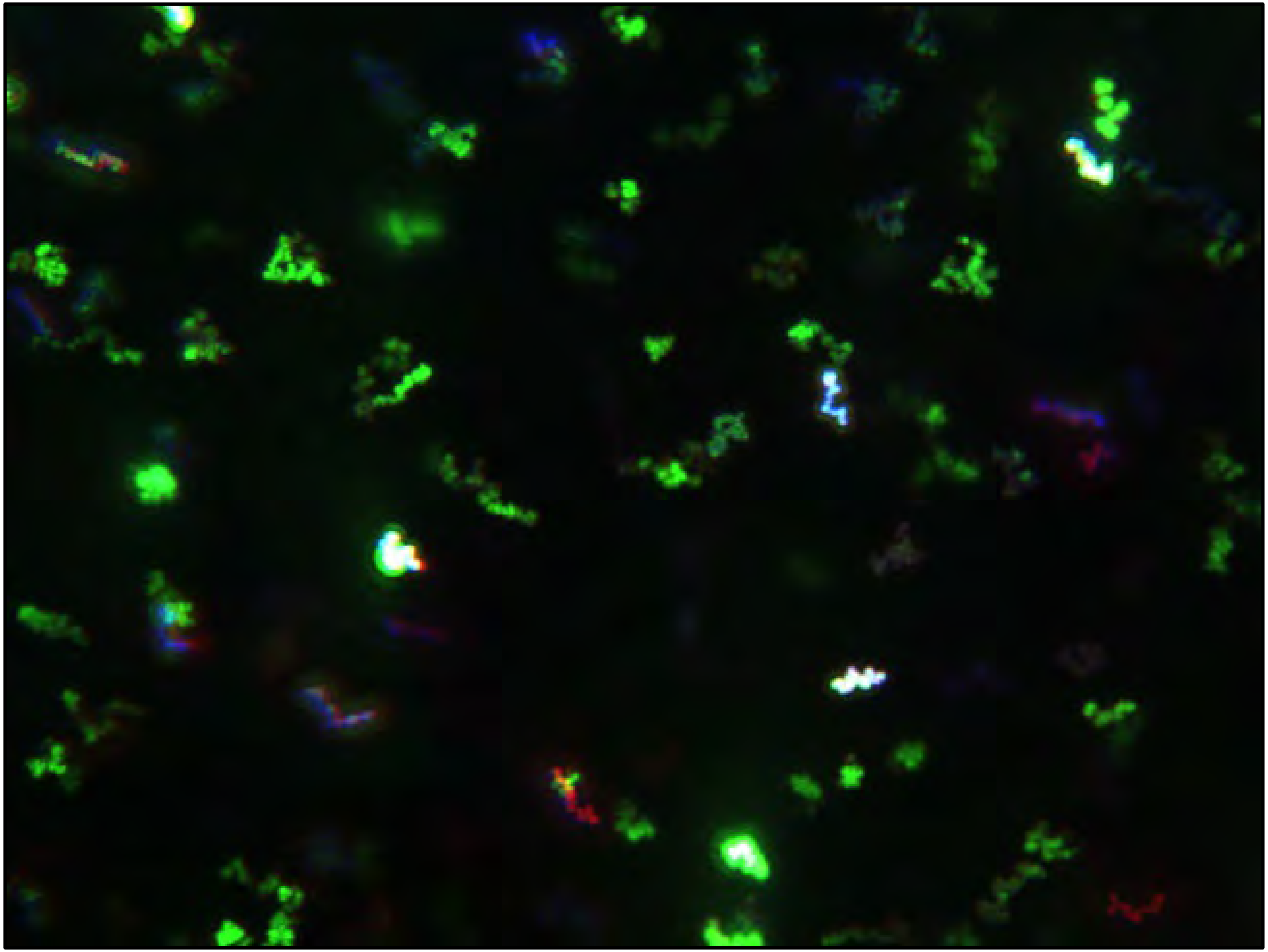

How can we account for large complexity of seawater composition?

Mineral particles

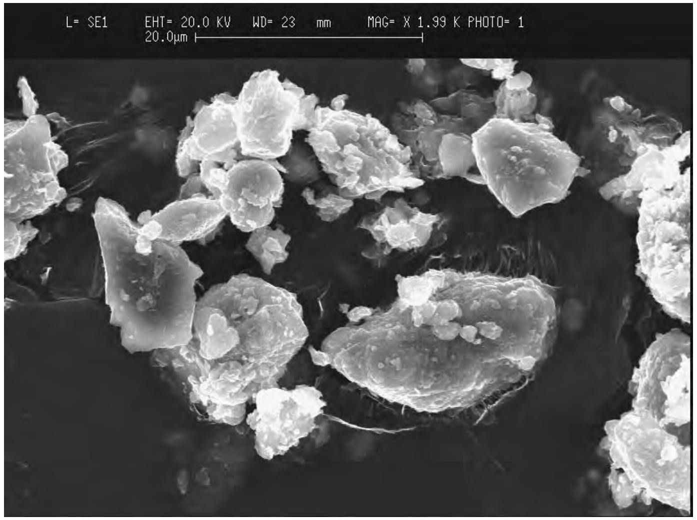

Plankton microorganisms

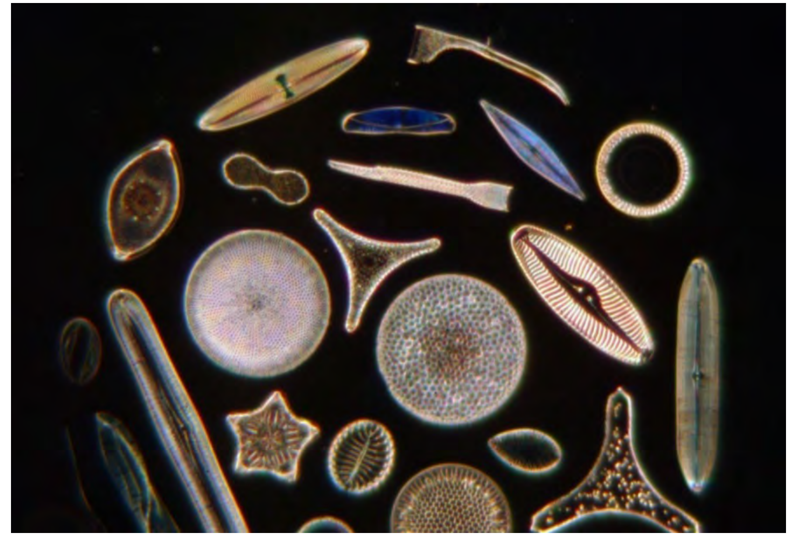

Colloids / nanoparticles

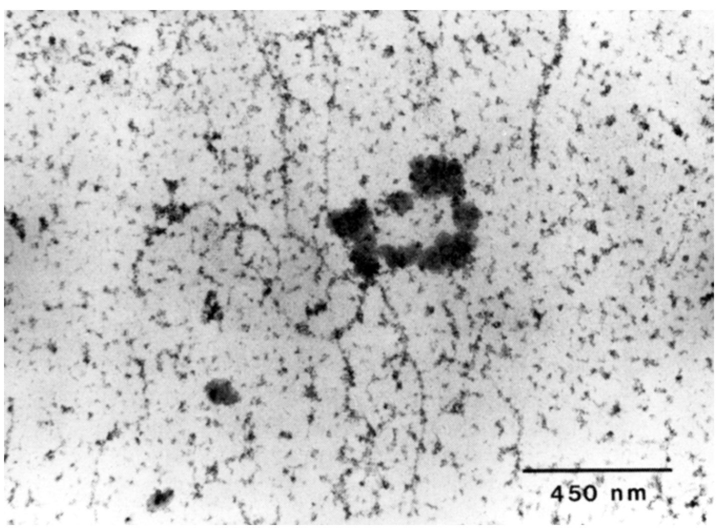

Linkage between single-particle and bulk optical properties of particle suspension

$$IOP(\lambda) = \sum_{i=1}^{\gg 1} (N/V)_i \, Q_i(\lambda) \, G_i = \sum_{i=1}^{\gg 1} (N/V)_i \, \sigma_i(\lambda)$$

$$\sigma_i(\lambda) = Q_i(\lambda) \, G_i = IOP_i(\lambda) \, / \, (N/V)_i$$

Bulk properties:

IOP – *a*, *b*, b_b, *c*, *VSF*

N/V – number concentration of particles

Single-particle properties:

Q – optical efficiency factor

G – geometric cross-section

σ – optical cross-section

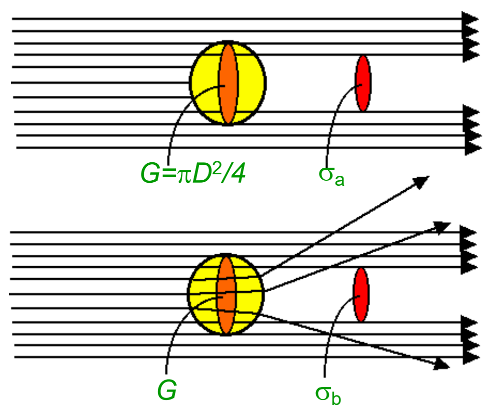

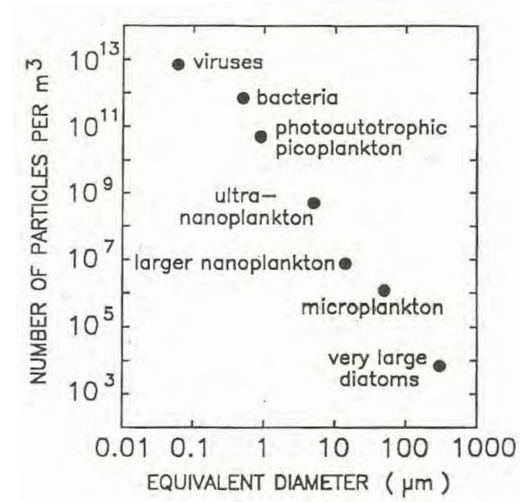

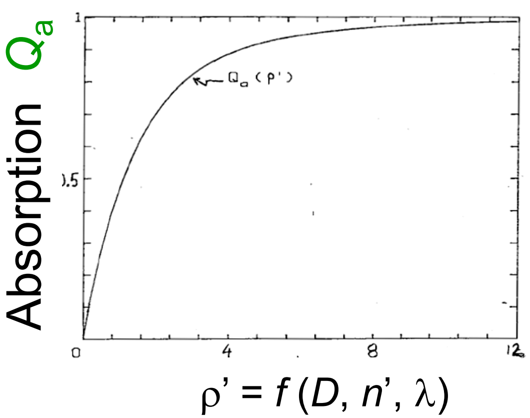

Morel and Bricaud (1981)

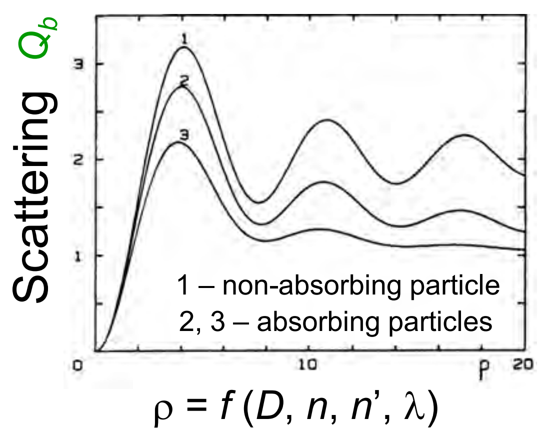

Morel and Bricaud (1986)

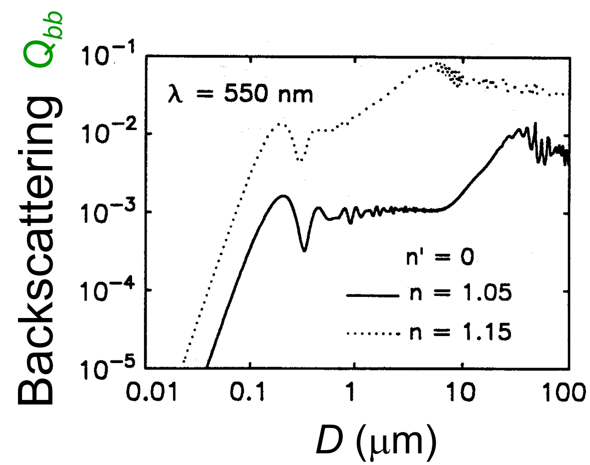

Stramski and Kiefer (1991)

Chlorophyll-based approach

Parameterization of seawater composition in terms of chlorophyll-a concentration alone

$$IOP(\lambda) = IOP_w(\lambda) + f\,[\ Chla\ ]$$

for example $a_{ph}(\lambda) = f\,[\ Chla\ ]$

$$a_p(\lambda) = f\,[\ Chla\ ]$$

$$AOP(\lambda)\ (e.g.,\ \text{ocean reflectance}) = f\,[\ Chla\ ]$$

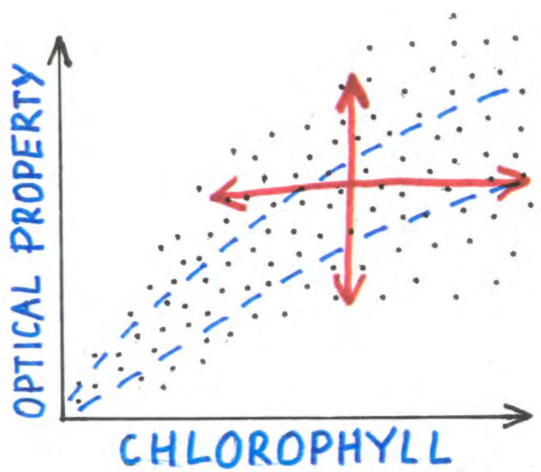

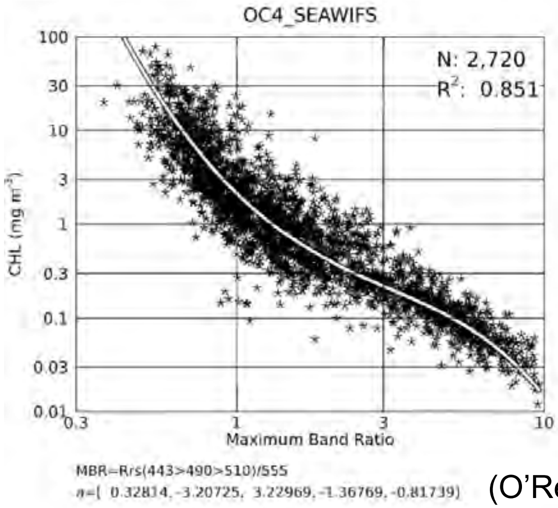

(O'Reilly & Werdell 2019)

Traditional approach with a few IOP components

Inherent Optical Properties (IOPs) are described in terms of a few broadly-defined categories of seawater constituents amenable to measurements

$$IOP(\lambda) = IOP_w(\lambda) + IOP_p(\lambda) + IOP_{CDOM}(\lambda)$$

$$IOP_p(\lambda) = IOP_{ph}(\lambda) + IOP_{NAP}(\lambda)$$

pure water (w), all particles (p), phytoplankton (ph), non-algal/detrital particles (NAP or d), chromophoric dissolved organic matter (CDOM or g)

Basic IOPs: absorption, scattering, and beam attenuation coefficients, volume scattering function

$$Ocean\ Color\ \ R_{rs}(\lambda) \propto \frac{b_b(\lambda)}{a(\lambda)} = \frac{b_{bw}(\lambda)+b_{bp}(\lambda)}{a_w(\lambda)+a_{ph}(\lambda)+a_d(\lambda)+a_g(\lambda)}$$

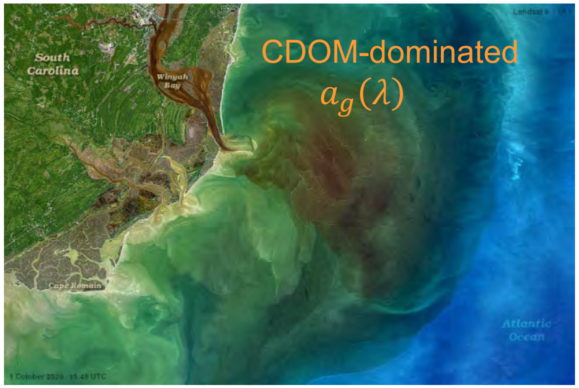

South Carolina coast, Landsat 8 , October 1, 2020 (NASA Ocean Color Web)

Halifax Bay, Eastern Australia
https://blogs.ntu.edu.sg/science/2020/06/24/lights-out-for-muddy-water-coral-reefs-as-global-sea-level-rises/

Phytoplankton-dominated

Coccolithophore bloom, Santa Barbara Channel (https://www.independent.com /2015/ 06/15/ chalk-producing-plankton-turn-ocean-turquoise/)

Microcystis bloom, Lake Erie, July 15, 2019 (https://ocj.com/2021/08/microcystis-cyanobacteria-bloom-monitoring-in-western-lakeerie/

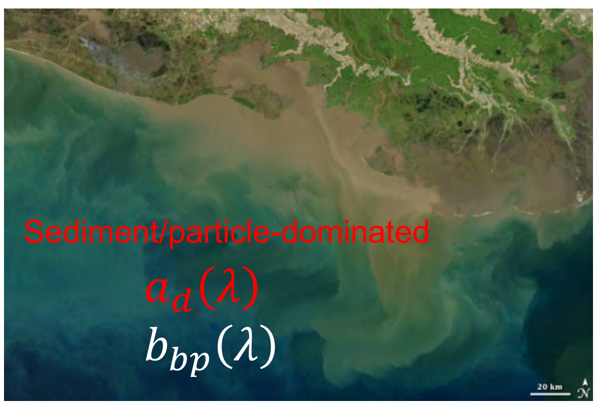

Atchafalaya River plume, Gulf of Mexico, MODIS-Aqua, April 7, 2009 (https://earthobservatory.nasa.gov/ images/ 38273/ sediment-in-the-gulf-of-Mexico)

Tijuana River plume, Imperial Beach, California (https://giddingslab.ucsd.edu/research/coastal-ocean/small-plume-dispersion/)

Lingulodinium bloom, off California coast (http://oceandatacenter.ucsc.edu /PhytoGallery/harmful-algae.html)

Reductionist approach

To develop an understanding and assemble a model of the whole, from the reductionist study of its parts

$$IOP_{\mathrm{p}}(\lambda) = \sum_{k} IOP_{k,\,pla}(\lambda) \quad \text{plankton}$$

$$+ \sum_{m} IOP_{m,\,min}(\lambda) \quad \text{minerals}$$

$$+ \sum_{n} IOP_{n,\,det}(\lambda) \quad \text{detritus}$$

Example IOP model with detailed description of plankton community

For example, for absorption we have:

$$a_{all} = \Sigma\, (N/V)_i\, (\sigma_a)_i$$

where the sum includes *all* species/groups of microorganisms and other particles, each denoted by subscript *i*

i	Component	Concentration [particles/m^3]	*Chl* [mg m^{-3}]
1	VIRU	$1.0 \cdot 10^{13}$	0
2	HBAC	$4.0 \cdot 10^{11}$	0
3	PROC	$7.0 \cdot 10^{10}$	0.1026
4	SYNE	$2.0 \cdot 10^{10}$	0.0403
5	SYMA	$8.0 \cdot 10^{9}$	0.0360
Σ	Picoplankton	$4.98 \cdot 10^{11}$	0.1789
6	PING	$4.5056 \cdot 10^{8}$	0.0540
7	PSEU	$0.9808 \cdot 10^{8}$	0.0303
8	LUTH	$0.9924 \cdot 10^{8}$	0.0107
9	GALB	$0.4839 \cdot 10^{8}$	0.0155
10	HUXL	$0.4339 \cdot 10^{8}$	0.0104
11	CRUE	$0.4496 \cdot 10^{8}$	0.0129
12	FRAG	$0.4768 \cdot 10^{8}$	0.0157
13	PARV	$0.6247 \cdot 10^{8}$	0.0181
14	BIOC	$0.3966 \cdot 10^{8}$	0.0900
15	TERT	$0.3570 \cdot 10^{8}$	0.0609
16	CURV	$0.2987 \cdot 10^{8}$	0.0099
Σ	Small Nanoplankton	$1.0 \cdot 10^{9}$	0.3284
17	ELON	$1.7 \cdot 10^{7}$	0.1595
18	MICA	$2.0 \cdot 10^{6}$	0.0508
Σ	Total Plankton	$1.0499019 \cdot 10^{13}$	0.7176
19	DET	$3.3 \cdot 10^{14}$	0
20	MIN	$1.1 \cdot 10^{14}$	0
Σ	Total Non-living Particles	$4.4 \cdot 10^{14}$	0
21	BUB	$7.1 \cdot 10^{6}$	0

(Stramski et al. 2001)

Size distribution

18 planktonic components
composite plankton
mineral particles
organic detritus
air bubbles

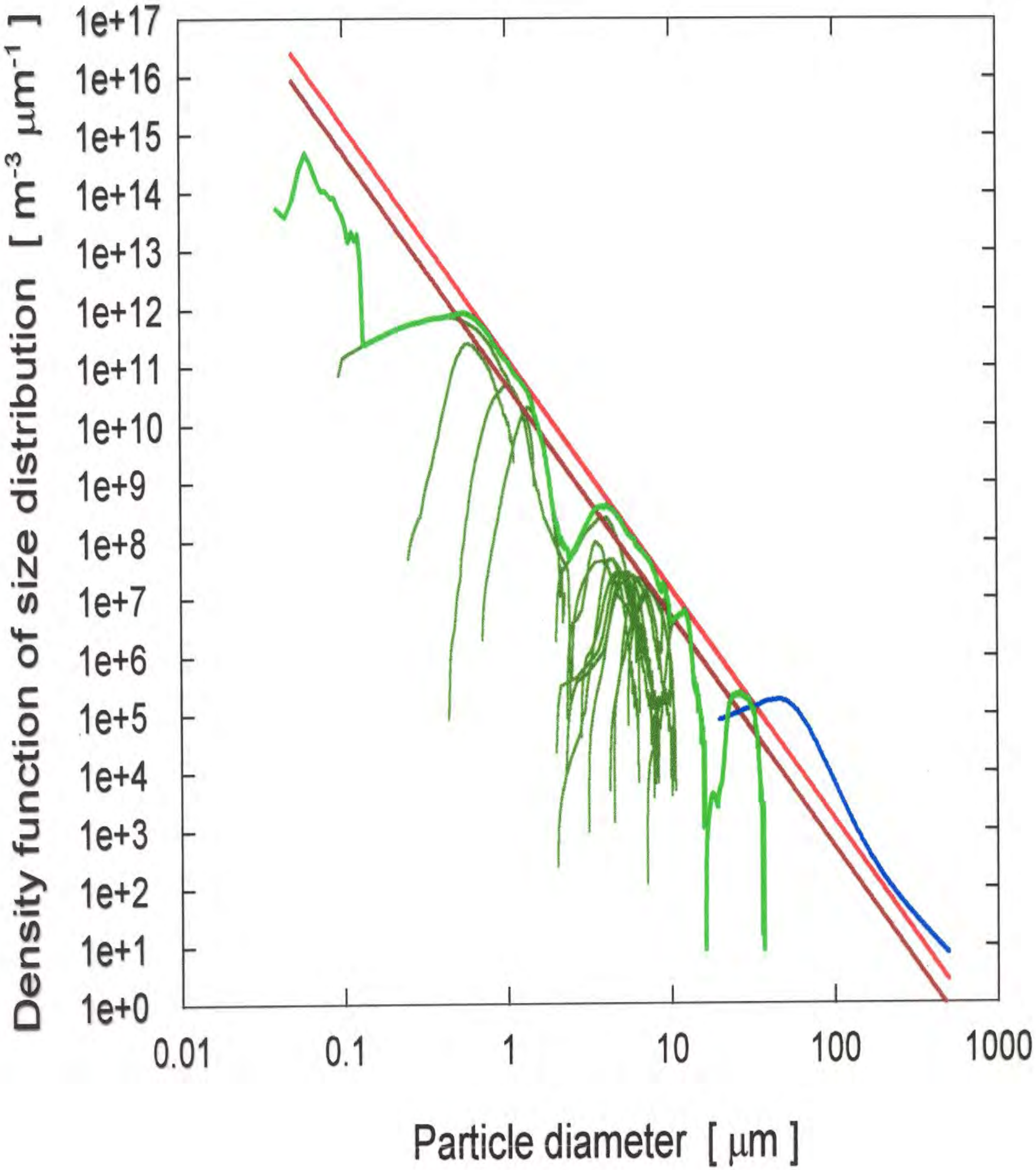

(Stramski et al. 2001)

Absorption budget

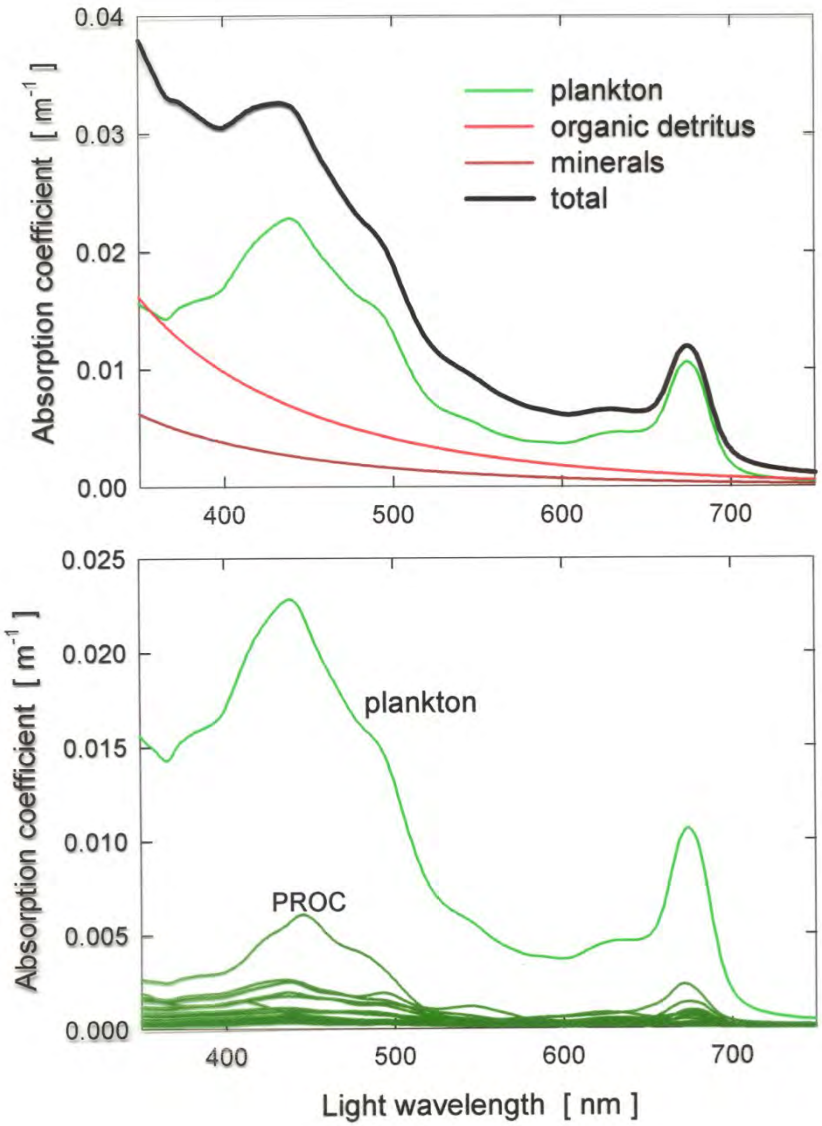

Scattering budget

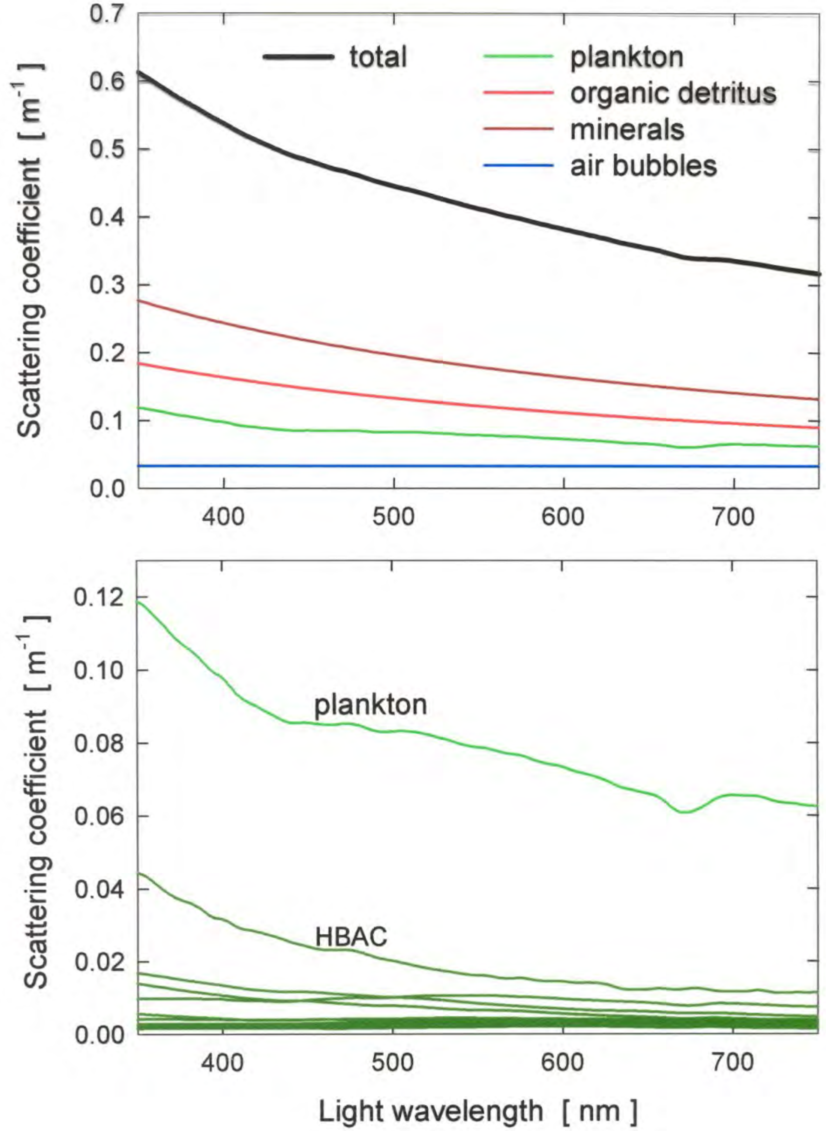

(Stramski et al. 2001)

Reductionist radiative transfer/reflectance model

Input to radiative transfer model

$$IOP(\lambda) = \sum_{i=1}^{j} IOP_i(\lambda) = \sum_{i=1}^{j} N_i \overline{\sigma_i}(\lambda)$$

Output, *e.g.* ocean reflectance

$$R(\lambda) = f\,[\sum_{i=1}^{j} N_\mathrm{i} \overline{\sigma}_{i,a}(\lambda), \sum_{i=1}^{j} N_\mathrm{i} \overline{\sigma}_{i,b}(\psi, \lambda)]$$

- In what ways does variability in detailed seawater composition determine variability in ocean reflectance?
- What information about water constituents and optical properties can we hope to extract from remotely sensed reflectance with acceptable accuracy?

Example combination of reductionist IOP model and radiative transfer model for simulating ocean color

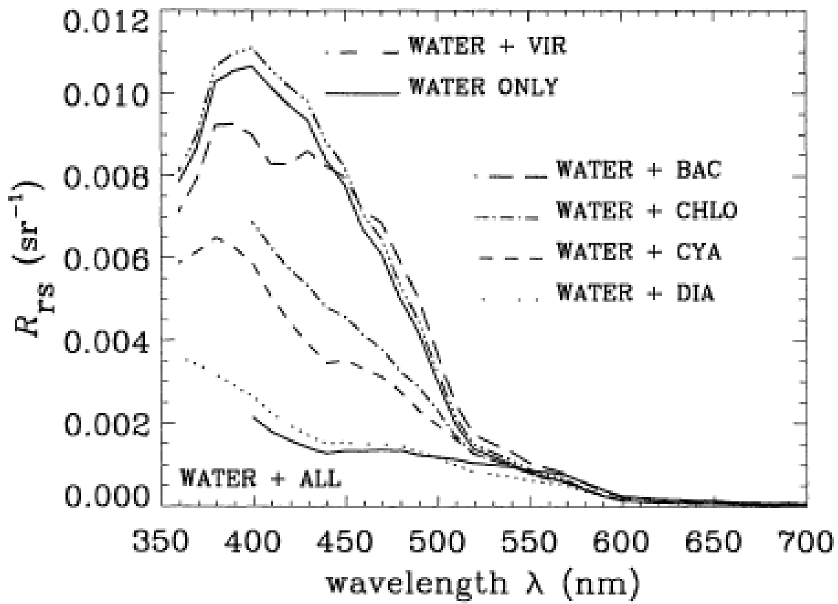

Viruses (~0.07 μm in size)
Heterotrophic bacteria (~0.5 μm)
Cyanobacteria (~1 μm)
Small diatoms (~4 μm)
Chlorophytes (~8 μm)
Detritus
CDOM

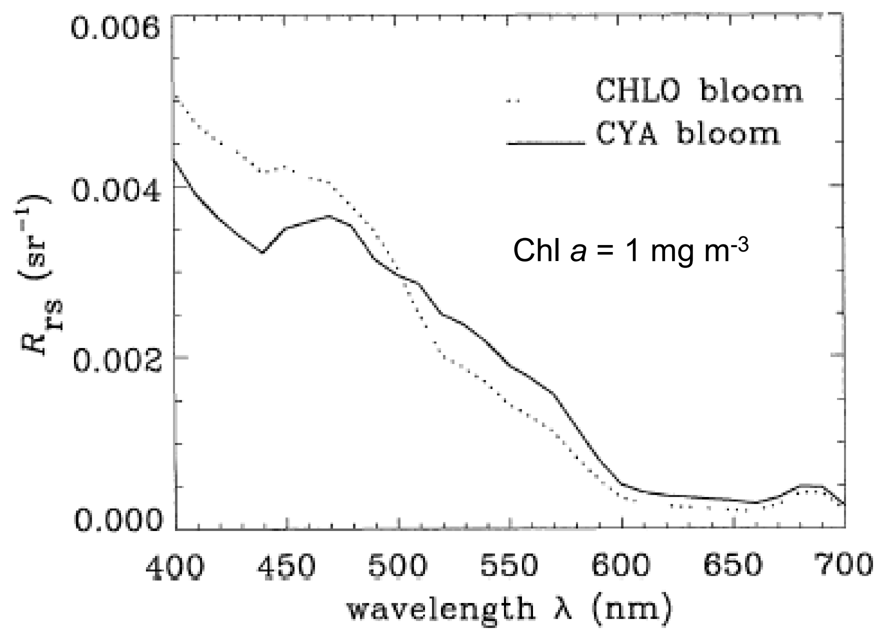

Stramski and Mobley (1997)
Mobley and Stramski (1997)

The complexity of seawater as an optical medium should not deter us from pursuing the proper course in future research

"The reductionist worldview has to be accepted as it is, not because we like it, but because that is the way the world works"

Steven Weinberg, Dreams of a Final Theory (1992)

1979 Nobel Prize in Physics